جامعة الملك عبدالله
للعلوم والتقنية
King Abdullah University of
Science and Technology

Direct and Energy-Transfer-Mediated Charge-Transfer State Formation and Recombination in Triangulene-Spacer-Perylenediimide Multichromophores: Lessons for Photovoltaic Applications

Item Type	Article
Authors	Albalawi, Ahmed;Stappert, Sebastian;Gorenflot, Julien;Li, Chen;Müllen, Klaus;Andrienko, Denis;Laquai, Frédéric
Citation	Balawi, A. H., Stappert, S., Gorenflot, J., Li, C., Müllen, K., Andrienko, D., & Laquai, F. (2019). Direct and Energy-Transfer-Mediated Charge-Transfer State Formation and Recombination in Triangulene-Spacer-Perylenediimide Multichromophores: Lessons for Photovoltaic Applications. The Journal of Physical Chemistry C, 123(27), 16602–16613. doi:10.1021/acs.jpcc.9b05149
Eprint version	Post-print
DOI	10.1021/acs.jpcc.9b05149
Publisher	American Chemical Society (ACS)
Journal	The Journal of Physical Chemistry C
Rights	This document is the Accepted Manuscript version of a Published Work that appeared in final form in The Journal of Physical Chemistry C, copyright © American Chemical Society after peer review and technical editing by the publisher. To access the final edited and published work see http://pubs.acs.org/doi/10.1021/acs.jpcc.9b05149.
Download date	2024-04-16 13:55:41
Link to Item	http://hdl.handle.net/10754/656098

Supporting Information

Direct and Energy-Transfer-Mediated Charge-Transfer State Formation and Recombination in Triangulene-Spacer-Perylenediimide Multichromophores: Lessons for Photovoltaic Applications

Ahmed Hesham Balawi,[1,#] Sebastian Stappert,[2,#] Julien Gorenflot,[1] Chen Li,[2,$] Klaus Müllen,[2,*] Denis Andrienko,[1,2,*] Frédéric Laquai[1,*]

[1]King Abdullah University of Science and Technology (KAUST), KAUST Solar Center, Physical Sciences and Engineering Division, Materials Science and Engineering Program, Thuwal 23955-6900, Kingdom of Saudi Arabia

[2]Max Planck Institute for Polymer Research, Ackermannweg 10, D-55128 Mainz, Germany

[$]present address: School of Environment and Civil Engineering, Dongguan University of Technology, No.1, Daxue Rd., Songshan Lake, Dongguan, Guangdong Province, P. R. China.

[#]A.H. Balawi and S. Stappert contributed equally to the work

*Corresponding authors: muellen@mpip-mainz.mpg.de; frederic.laquai@kaust.edu.sa; denis.andrienko@mpip-mainz.mpg.de

Supplementary Note 1. SYNTHESIS

4,4,8,8,12,12-Hexamethyl-2,6-bis(4-(methylthio)phenyl)-8,12-dihydro-4H-benzo[9,1]quinolizino[3,4,5,6,7-defg]acridine (3)

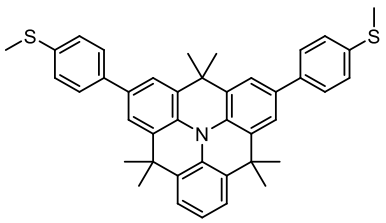

4-Methylthio phenylboronicacid pinacolester (40 mg, 0.161 mmol), 2,6-dibromo-4,4,8,8,12,12-hexamethyl-8,12-dihydro-4H-benzo[9,1]quinolizino-[3,4,5,6,7-*defg*]acridine (2) (140 mg, 0.268 mmol) were dissolved in 1,4-dioxane (10 mL). Additionally, K_2CO_3 (739 mg, 5.35 mmol) and water (3 mL) were added. The solution was degased by argon-bubbling for 30 minutes before $Pd(PPh_3)_4$ (31 mg, 0.1 eq) was added. The mixture was stirred for 4 hours at 90 °C, then the solvent was removed under reduced pressure and the remaining solid was subjected to flash-silica gel column chromatography (DCM/PE, 1:1). The obtained product 3 was then precipitated from DCM/MeOH, yielding 3 as a white solid (142 mg, 87%).

^{1}H-NMR (300 MHz, CD_2Cl_2) δ [ppm] = 7.65 – 7.62 (m, 6H), 7.61 (s, 2H), 7.44 (d, J = 7.7 Hz, 2H), 7.36 (d, J = 8.4 Hz, 4H), 7.16 (t, J = 7.8 Hz, 1H), 2.54 (s, 6H), 1.75 (s, 6H), 1.70 (s, 12H).

^{13}C-NMR (75 MHz, CD_2Cl_2) δ [ppm] = 138.37, 135.22, 131.04, 130.43, 127.51, 127.40, 124.27, 123.73, 122.51, 36.24, 33.63, 16.35.

FD-MS (8kV): m/z = (M+) 610.1 (100%).

Elemental Analysis:

Calculated (%) C: 80.74, H: 6.45, N: 2.30, S: 10.51;

Experimental (%) C: 80.64, H: 6.43, N: 2.20, S: 10.53.

FT-IR: $\tilde{\nu}$ [cm^{-1}] = 742, 764, 792, 817, 880, 968, 1014, 1063, 1098, 1127, 1213, 1290, 1301, 1316, 1436, 2854, 29220, 2965, 3023.

MP.: 183 °C.

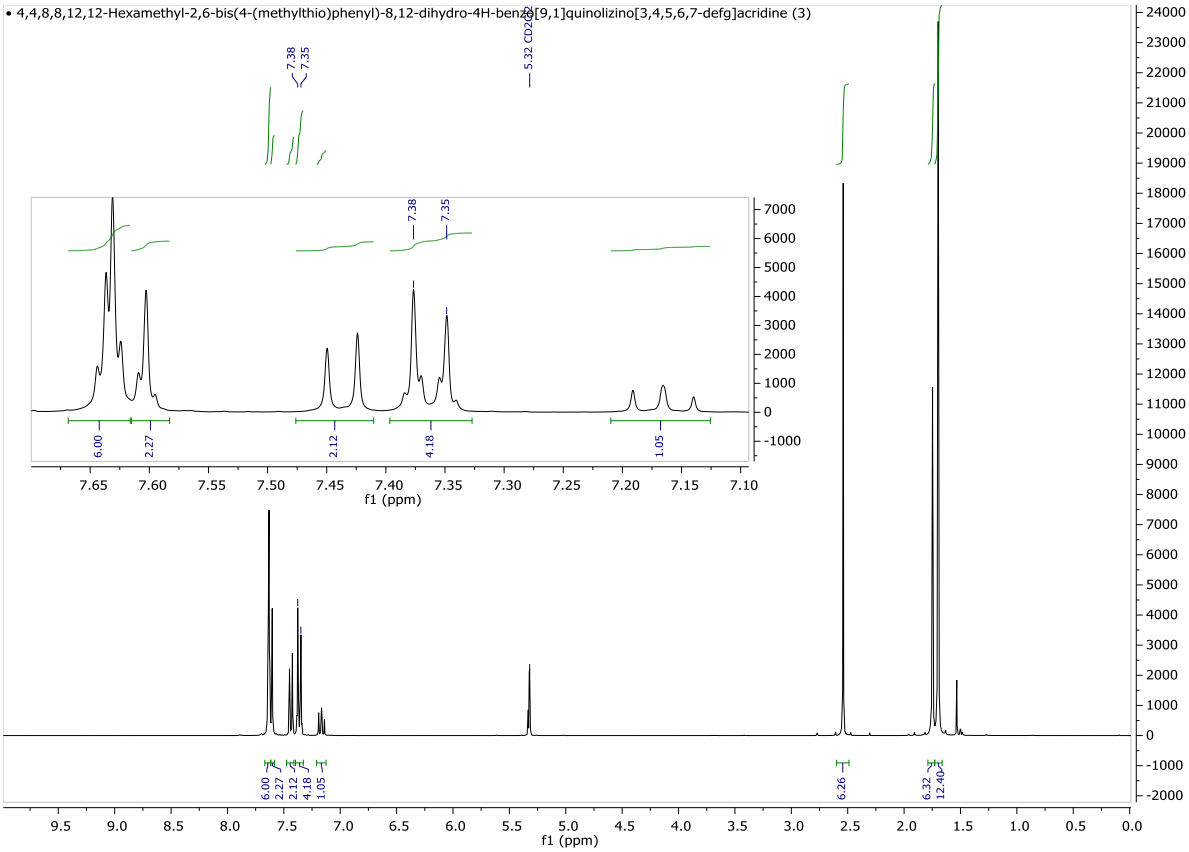
• 4,4,8,8,12,12-Hexamethyl-2,6-bis(4-(methylthio)phenyl)-8,12-dihydro-4H-benzo[9,1]quinolizino[3,4,5,6,7-defg]acridine (3)
7.38
7.35
5.32 CD2Cl2
6.00
2.27
2.12
4.18
1.05
6.26
6.32
12.40
f1 (ppm)

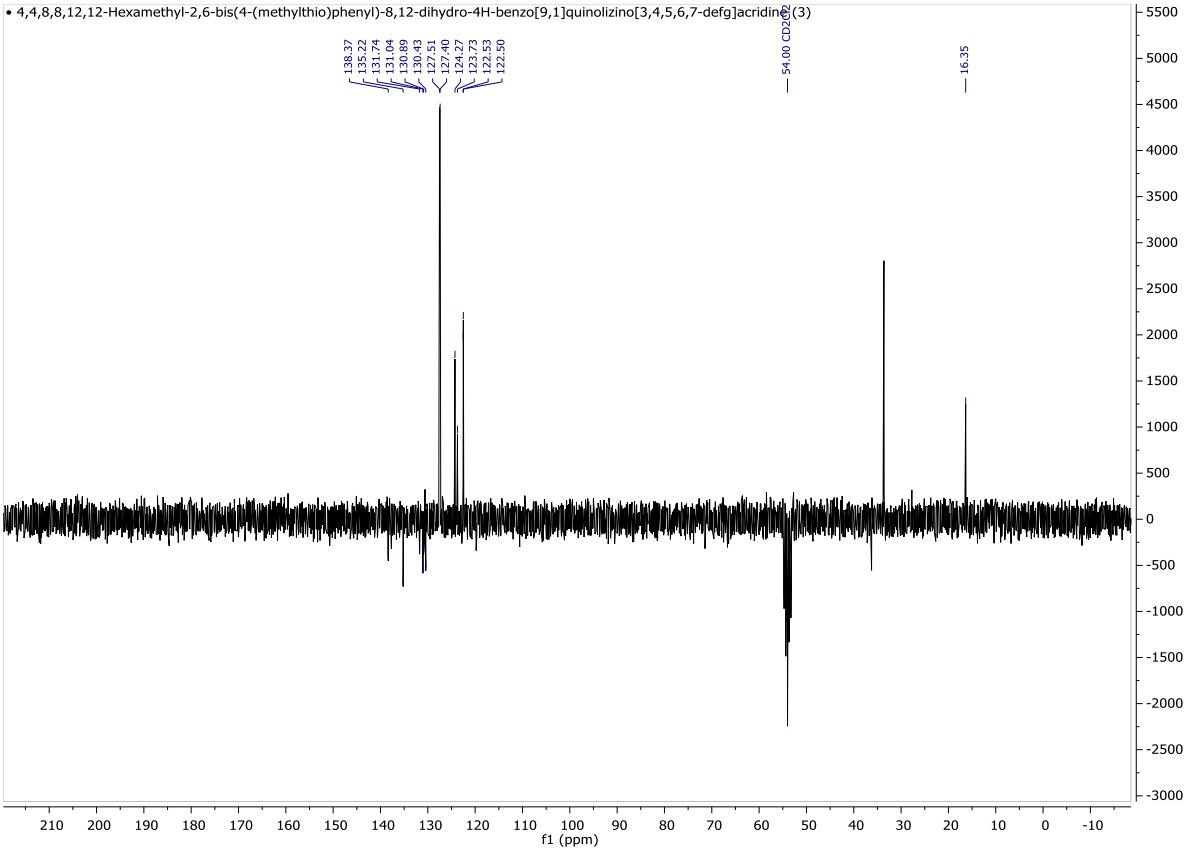
• 4,4,8,8,12,12-Hexamethyl-2,6-bis(4-(methylthio)phenyl)-8,12-dihydro-4H-benzo[9,1]quinolizino[3,4,5,6,7-defg]acridine (3)
138.37
135.22
131.74
131.04
130.89
130.43
127.51
127.40
124.27
123.73
122.53
122.50
54.00 CD2Cl2
16.35
f1 (ppm)

2-Bromo-4,4,8,8,12,12-hexamethyl-6,10-bis(4-(methylthio)phenyl)-8,12-dihydro-4H-benzo[9,1]quinolizino[3,4,5,6,7-defg]acridine (4)

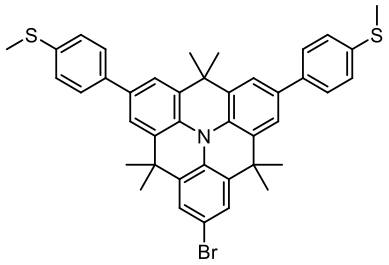

4,4,8,8,12,12-Hexamethyl-2,6-bis(4-(methylthio)phenyl)-8,12-dihydro-4H-benzo[9,1]-quinolizino[3,4,5,6,7-defg]acridine (3) (102 mg, 0.167 mmol) was dissolved in chloroform (20 mL) and cooled in an ice-bath. Under the exclusion of light, NBS (30 mg, 0.167 mmol) was added in one portion. The mixture was stirred at 0 °C for two hours. Since product and starting material showed identical elution behavior on TLC, reaction turnover had to be quantitative, which was monitored by FD-MS. The organic phase was extracted with aqueous sodium sulfite solution. The chloroform phase was then evaporated to dryness. The obtained yellow oil was dissolved in DCM, then put into the double amount of methanol. Reducing the total amount of solvent to approx. half amount via rotary evaporation and subsequent cooling to 0 °C to yield the product as an analytically pure, white powder (163 mg, 76%).

^{1}H-NMR (250 MHz, CD_2Cl_2) δ [ppm] = 7.66 – 7.56 (m, 8H), 7.51 (s, 2H), 7.36 (d, J = 8.5 Hz, 4H), 2.54 (s, 6H), 1.75 (s, 6H), 1.67 (s, 12H).

^{13}C-NMR (75 MHz, CD_2Cl_2) δ [ppm] = 138.19, 135.62, 131.09, 130.60, 127.50, 127.42, 126.93, 122.83, 122.46, 36.41, 33.87, 33.33, 16.32.

FD-MS (8kV): m/z = (M+) 689.0 (100%).

Elemental Analysis:

Calculated (%) C: 71.50, H: 5.56, N: 2.03, S: 9.31,

Experimental (%) C: 70.43, H: 5.83, N: 1.93, S: 9.40.

FT-IR: $\tilde{\nu}$ [cm^{-1}] = 506, 523, 555, 588, 632, 668, 704, 736, 755, 766, 818, 858, 879, 955, 968, 1014, 1062, 1098, 1121, 1208, 1286, 1301, 1314, 1437, 1599, 2856, 2919, 2970, 3022, 3042, 3073.

MP.: 247 °C.

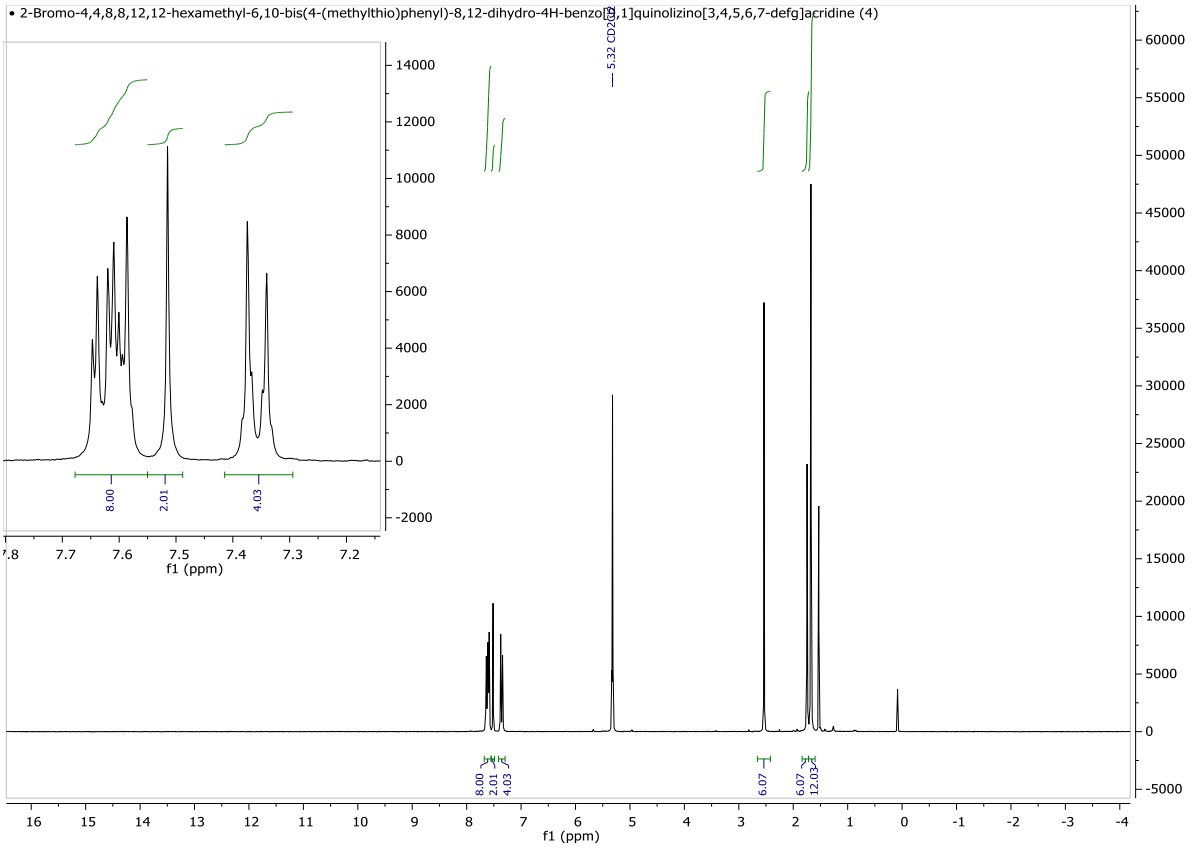
• 2-Bromo-4,4,8,8,12,12-hexamethyl-6,10-bis(4-(methylthio)phenyl)-8,12-dihydro-4H-benzo[9,1]quinolizino[3,4,5,6,7-defg]acridine (4)
5.32 CD2Cl2
8.00
2.01
4.03
6.07
6.07
12.03
f1 (ppm)

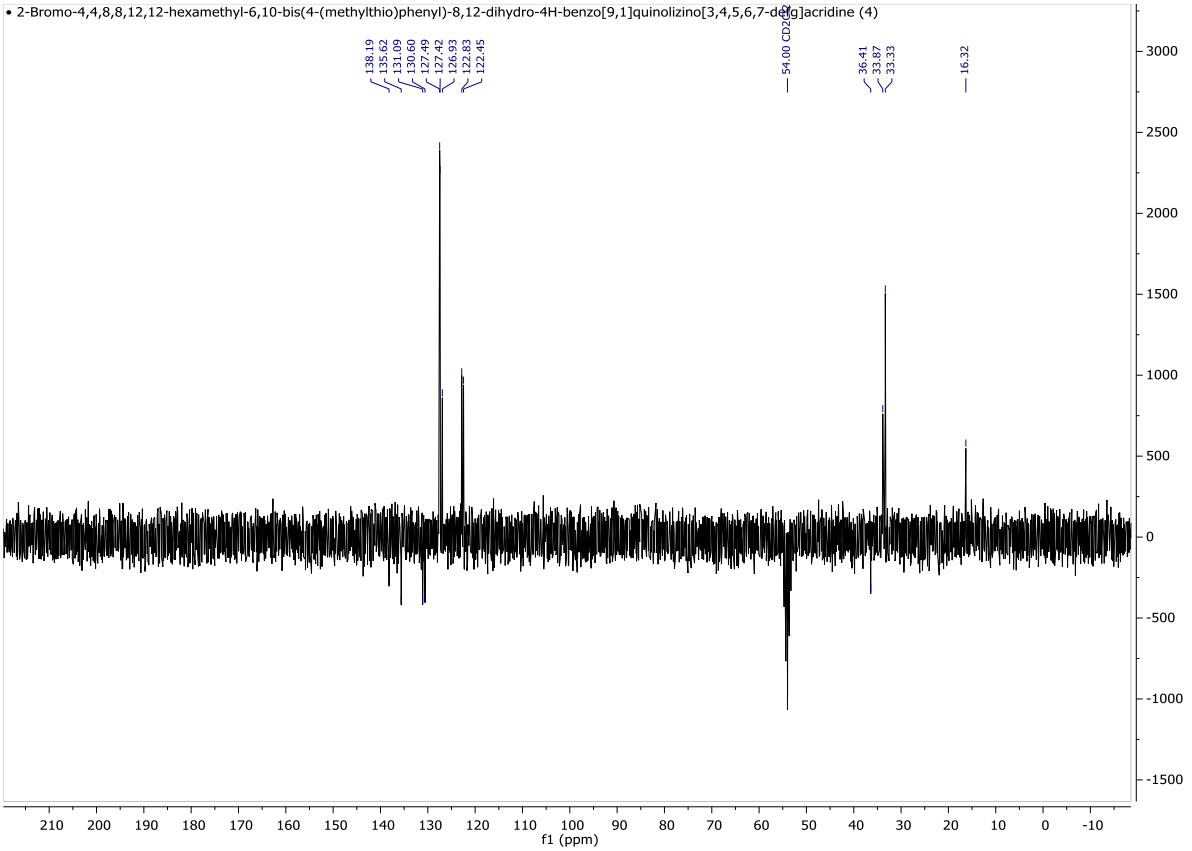
• 2-Bromo-4,4,8,8,12,12-hexamethyl-6,10-bis(4-(methylthio)phenyl)-8,12-dihydro-4H-benzo[9,1]quinolizino[3,4,5,6,7-defg]acridine (4)
138.19
135.62
131.09
130.60
127.49
127.42
126.93
122.83
122.45
54.00 CD2Cl2
36.41
33.87
33.33
16.32
f1 (ppm)

Dimethyl-2-(10H-phenothiazin-10-yl)isophthalate (7)

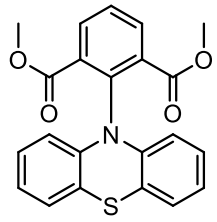

Dimethyl-2-bromoisophthalate (32.0 g, 117.2 mmol), phenothiazine (6) (23.4 g, 117.2 mmol), copper powder (0.74 g, 11.7 mmol), copper(I) iodide (15.6 g, 82.0 mmol) and potassium carbonate (45.6 g, 351.5 mmol) were suspended in diphenylether (500 mL) under argon atmosphere. The flask was evacuated and flushed with argon three times before the mixture was stirred at 190 °C over 2 days. The mixture was filtered through a paper filter while still warm. The filtrate with diphenylether was then subjected to silica gel column chromatography (PE/DCM, 1:0 to 1:1). Remaining diphenylether was washed out with petroleum ether, then dichloromethane was added as more polar eluent. The product was obtained as a pale yellow solid (33.6 g, 73%) that quickly turned green when stored under ambient atmosphere.

^{1}H-NMR (500 MHz, CD_2Cl_2) δ [ppm] = 8.23 (d, *J* = 7.8 Hz, 2H), 7.69 (t, *J* = 7.8 Hz, 1H), 6.99 – 6.82 (m, 2H), 6.76 (ddd, *J* = 6.3, 3.8, 1.9 Hz, 4H), 5.96 – 5.60 (m, 2H), 3.74 (s, 6H).

^{13}C-NMR (126 MHz, CD_2Cl_2) δ [ppm] = 166.01, 143.32, 139.08, 135.94, 134.96, 129.65, 127.16, 126.74, 122.64, 119.29, 115.53, 53.15.

FD-MS (8kV): m/*z* = (100%) 391.0 [M^+].

Elemental Analysis:

Calculated (%) C: 67.50, H: 4.38, N: 3.58, S: 8.19,

Experimental (%) C: 66.74, H: 4.38, N: 3.48, S: 8.16.

FT-IR: $\tilde{\nu}$ [cm^{-1}] = 744, 994, 1045, 1093, 1120, 1153, 1207, 1258, 1280, 1317, 1434, 1466, 1489, 1576, 1589, 1718, 1735, 2950, 3010, 3069.

MP.: 169 °C.

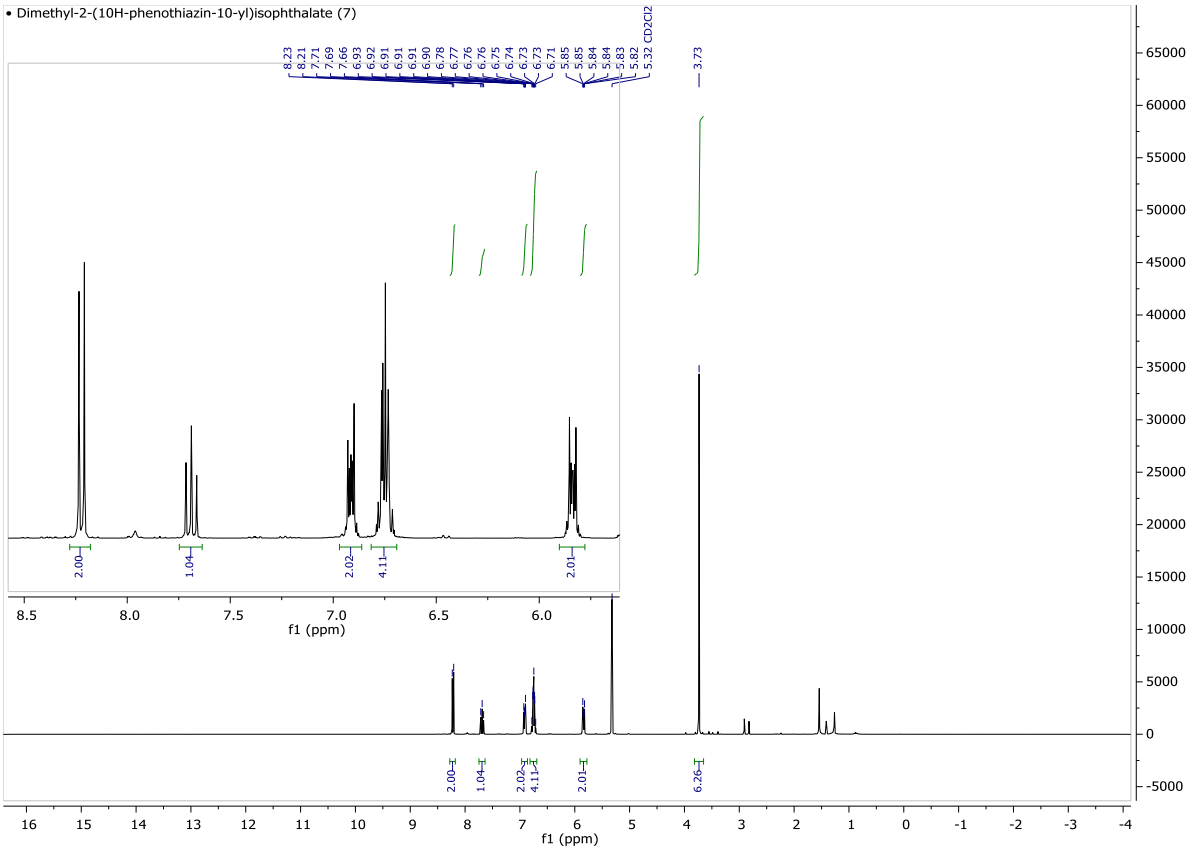
• Dimethyl-2-(10H-phenothiazin-10-yl)isophthalate (7)
8.23
8.21
7.71
7.69
7.66
6.93
6.92
6.91
6.91
6.90
6.78
6.77
6.76
6.76
6.75
6.74
6.73
6.73
6.71
5.85
5.85
5.84
5.84
5.83
5.82
5.32 CD2Cl2
3.73
2.00
1.04
2.02
4.11
2.01
f1 (ppm)
2.00
1.04
2.02
4.11
2.01
6.26
f1 (ppm)

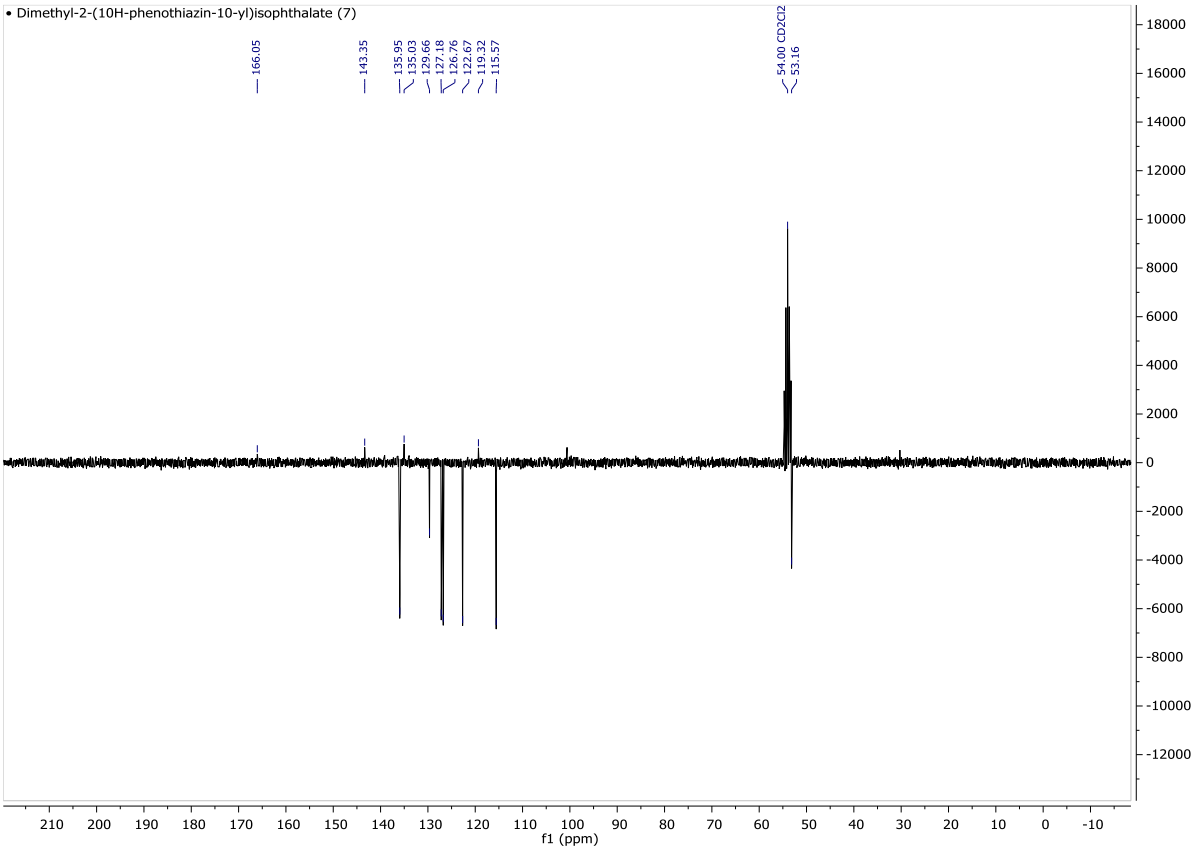
• Dimethyl-2-(10H-phenothiazin-10-yl)isophthalate (7)
166.05
143.35
135.95
135.03
129.66
127.18
126.76
122.67
119.32
115.57
54.00 CD2Cl2
53.16
f1 (ppm)

2,2'-(2-(10H-Phenothiazin-10-yl)-1,3-phenylene)bis(propan-2-ol) (8)

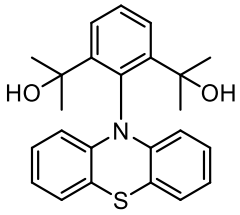

Dimethyl-2-(10*H*-phenothiazin-10-yl)*iso*phthalate (7) (33.6 g, 88.8 mmol) was weighed into a three-neck round-bottom flask and thoroughly evacuated. Under argon atmosphere, dry toluene (400 mL) and dry THF (400 mL) were added. Commercial methylmagnesium bromide (430 mL, 3 M in diethylether, 1.29 mol) was added through a dropping funnel over the period of 2 hours. After the addition of approx. 50 mL of MeMgBr, heating was started (45 °C). After complete addition, the temperature was raised to reflux (85 – 100 °C). The mixture was stirred continuesly for 2 days.

The mixture was poured onto 1.5 L of crushed ice while manual stirring was ensured. Concentrated hydrochloric acid was added in small amounts while ice was still visibly floating in the mixture. After dissolution of ice, external cooling was proceeded in an ice-bath. Addition of hydrochloric acid was continued until the aqueous phase was neutral, indicated by dissolution of the inorganic Mg-salts. The aqueous phase was separated and additionally extracted with ethylacetate (5 times 350 mL) and an additional time with dichloromethane (400 mL). The combined organic phases were dried over $MgSO_4$, then evaporated to dryness. The obtained solid was directly used in the next step without any purification. The compound was directly converted, otherwise side reactions took place if not stored at -20 °C.

FD-MS (8kV): m/z = (100%) 392.8 [M^+].

8,8,12,12-Tetramethyl-8,12-dihydrobenzo[9,1]quinolizino[3,4,5,6,7-klmn]-phenothiazine, thio-spacerd N-heterotriangulene (9)

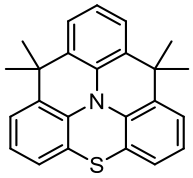

2,2'-(2-(10*H*-Phenothiazin-10-yl)-1,3-phenylene)bis(propan-2-ol) (8) (approx. 35 g, crude compound) was crushed to fine powder, then suspended in concentrated phosphoric acid (200 mL). Vigorous stirring by a mechanical stirrer was continued for 1 to 2 days. The obtained dark brownish solution was poured onto 1

L of crushed ice. Diluted NaOH solution was added in small portions while external cooling in an ice-bath was ensured. The slushy mixture was extracted with ethyl acetate (5 times 300 mL) and an additional time with dichloromethane (400 mL). The combined organic solvents were removed under reduced pressure. The obtained yellow solid was subjected to silica gel column chromatography (PE/DCM, 10:2) yielding pure product 9 as pale yellow solid (12.8 g, 42% over two steps).

^{1}H-NMR (500 MHz, CD_2Cl_2) δ [ppm] = 7.35 (d, J = 7.6 Hz, 2H), 7.19 (dd, J = 7.9, 1.7 Hz, 2H), 7.13 (t, J = 7.7 Hz, 1H), 6.92 (t, J = 7.6 Hz, 2H), 6.78 (dd, J = 7.4, 1.7 Hz, 2H), 1.57 (s, 12H).

^{13}C-NMR (126 MHz, CD_2Cl_2) δ [ppm] = 134.70, 132.25, 131.54, 130.15, 124.78, 124.77, 124.59, 123.96, 123.82, 116.67, 35.88, 33.03.

FD-MS (8kV): m/z = 355.7 (100%) [M^+].

Elemental Analysis:

Calculated (%) C: 81.09, H: 5.95, N: 3.94, S: 9.02,

Experimental (%) C: 80.85, H: 5.97, N: 4.05, S: 8.97.

FT-IR: $\tilde{\nu}$ [cm^{-1}] = 729, 744, 779, 897, 977, 1075, 1114, 1124, 1135, 1214, 1263, 1274, 1307, 1423, 2866, 2930, 2969.

MP.: 191 °C.

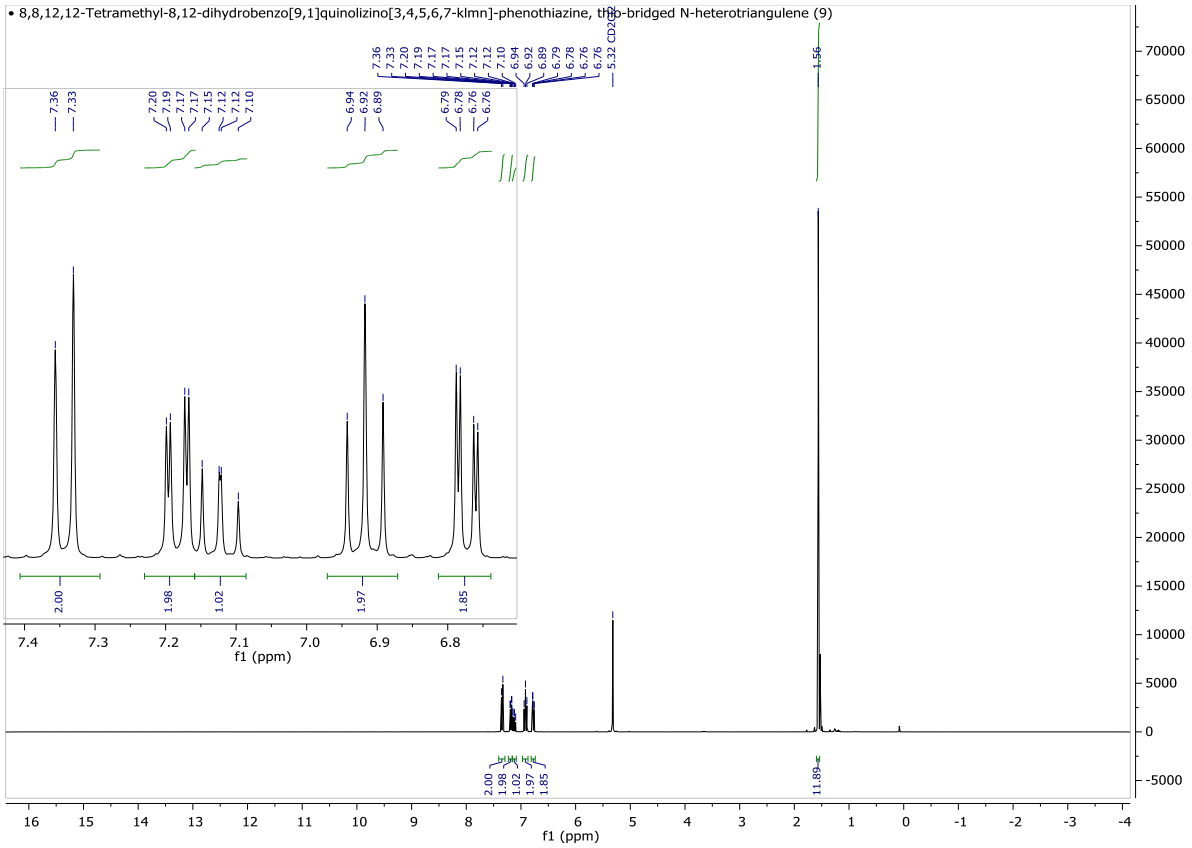

10-Bromo-8,8,12,12-tetramethyl-8,12-dihydrobenzo[9,1]quinolizino[3,4,5,6,7-klmn]-phenothiazine (10)

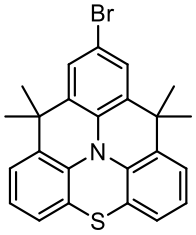

8,8,12,12-Tetramethyl-8,12-dihydrobenzo[9,1]quinolizino[3,4,5,6,7-*klmn*]-phenothia-zine (9) (1.00 g, 2.81 mmol) was dissolved in chloroform (200 mL). The flask was covered with alumina foil and suspended into an ice-bath. NBS (1.00 g, 2.81 mmol) was dissolved in a mixture of chloroform and THF (70+15 mL) which was then added to the cooled solution of 9 dropwise over the course of 30 minutes. Stirring was continued for one hour or up to overnight. The solution was extracted with sodium sulfite solution (2*100 mL), the organic phase was dried over $CaCl_2$ and subsequently evaporated to dryness. The solid was recrystallized from ethanol to obtain product 10 as crystalline, pale yellow compound (1.15 g, 94%).

^{1}H-NMR (500 MHz, CD_2Cl_2) δ [ppm] = 7.43 (s, 2H), 7.17 (dd, *J* = 7.9, 1.7 Hz, 2H), 6.93 (t, *J* = 7.6 Hz, 2H), 6.78 (dd, *J* = 7.4, 1.6 Hz, 2H), 1.55 (s, 12H).

^{13}C-NMR (126 MHz, CD_2Cl_2) δ [ppm] = 134.20, 132.44, 131.84, 131.18, 126.61, 125.08, 124.78, 124.67, 116.93, 116.33, 36.05, 32.79.

FD-MS (8kV): m/*z* = 434.2 (100%) [M^+].

FT-IR: $\tilde{\nu}$ [cm^{-1}] = 729, 757, 775, 859, 1097, 1125, 1145, 1206, 1278, 1421, 2873, 2925, 2970.

MP.: 179 °C.

HR MALDI-TOF MS (DCTB): *m/z* = 433.0479 calc. for $C_{24}H_{20}BrNS$: 433.0500.

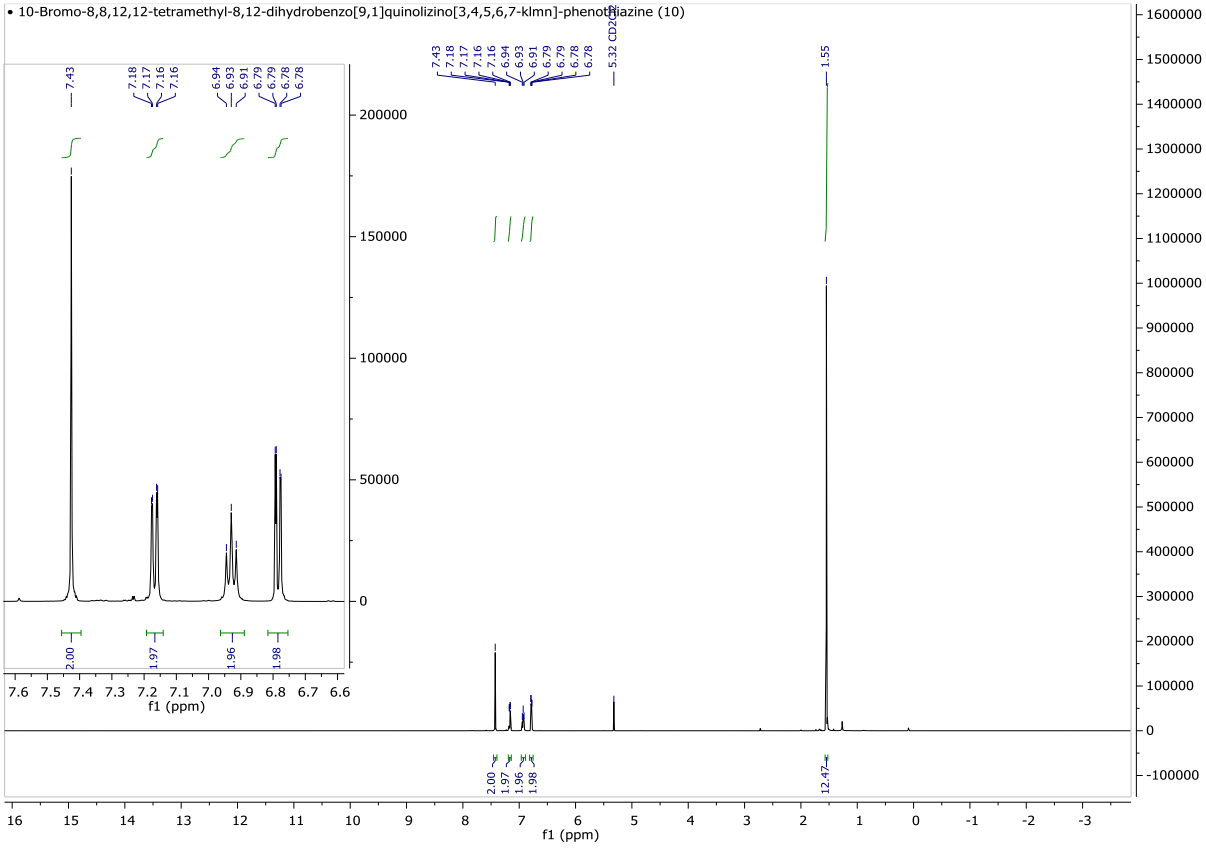

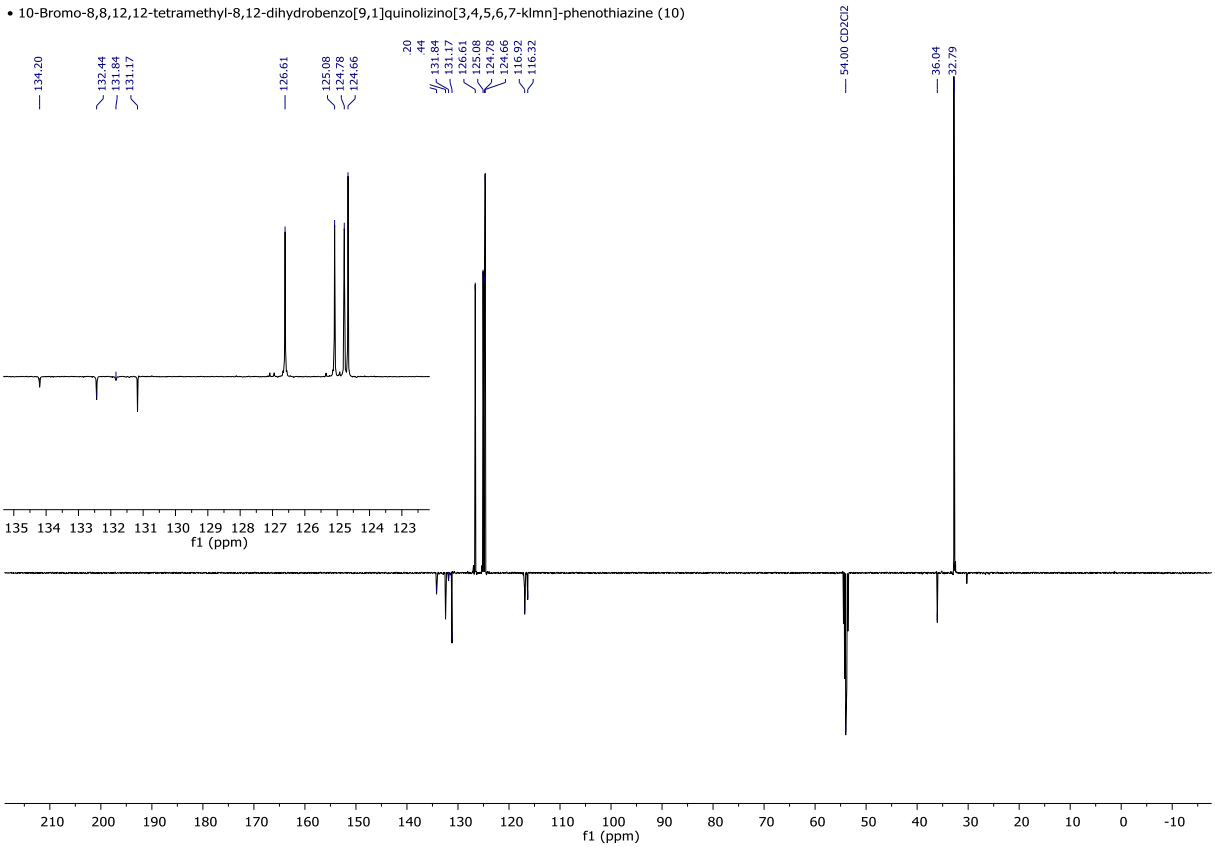

8,8,12,12-Tetramethyl-10-(4,4,5,5-tetramethyl-1,3,2-dioxaborolan-2-yl)-8,12-dihydrobenzo[9,1]quinolizino[3,4,5,6,7-klmn]phenothiazine (11)

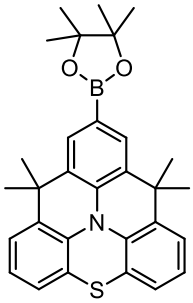

Monobromo *N*-heterotriangulene 10 (500 mg, 1.15 mmol), KOAc (407 mg, 4.14 mmol), and bis(pinacolato)diboron (365 mg, 1.44 mmol) were dissolved in 50 mL of dry DMF. After 30 minutes of argon bubbling, $Pd(dppf)Cl_2$ (38 mg, 0.046 mmol) was added and the mixture stirred under argon atmosphere at 85 °C for three hours. After completion the solvent was removed under reduced pressure and the black residue extracted with water and dichloromethane. The compound was purified by column chromatography on silica gel (petroleum ether/dichloromethane, 1:1). After removing the solvent, the

product was obtained as yellow, waxy compund. The product was dissolved in a small amount of dichloromethane, which was added to approx. 50 mL of methanol. The mixture was then sonicated for a few seconds until the product precipitated as a pale yellow powder (375 mg, 68%).

^{1}H-NMR (300 MHz, CD_2Cl_2) δ [ppm] = 7.73 (s, 2H), 7.20 (dd, *J* = 7.8, 1.7 Hz, 2H), 6.94 (t, *J* = 7.6 Hz, 2H), 6.78 (dd, *J* = 7.4, 1.7 Hz, 2H), 1.58 (s, 12H), 1.36 (s, 12H).

^{13}C-NMR (75 MHz, CD_2Cl_2) δ [ppm] = 134.84, 134.21, 132.20, 130.30, 129.07, 125.01, 124.73, 124.61, 116.94, 84.18, 35.84, 32.98, 25.28.

Elemental Analysis:

Calculated (%) C: 74.84, H: 6.70, N: 2.91, S: 6.66.

Experimental (%) C: 75.68, H: 5.75, N: 2.90, S: 7.44.

FT-IR: $\tilde{\nu}$ [cm^{-1}] = 688, 731, 765, 778, 855, 892, 967, 1104, 1127, 1144, 1207, 1278, 1297, 1356, 1380, 1420, 1436, 2869, 2927, 2976, 3070.

MP.: 97 °C.

HR MALDI-TOF MS (DCTB): *m/z* = 481.2263 calc. for $C_{30}H_{32}BNO_2S$: 481.2247.

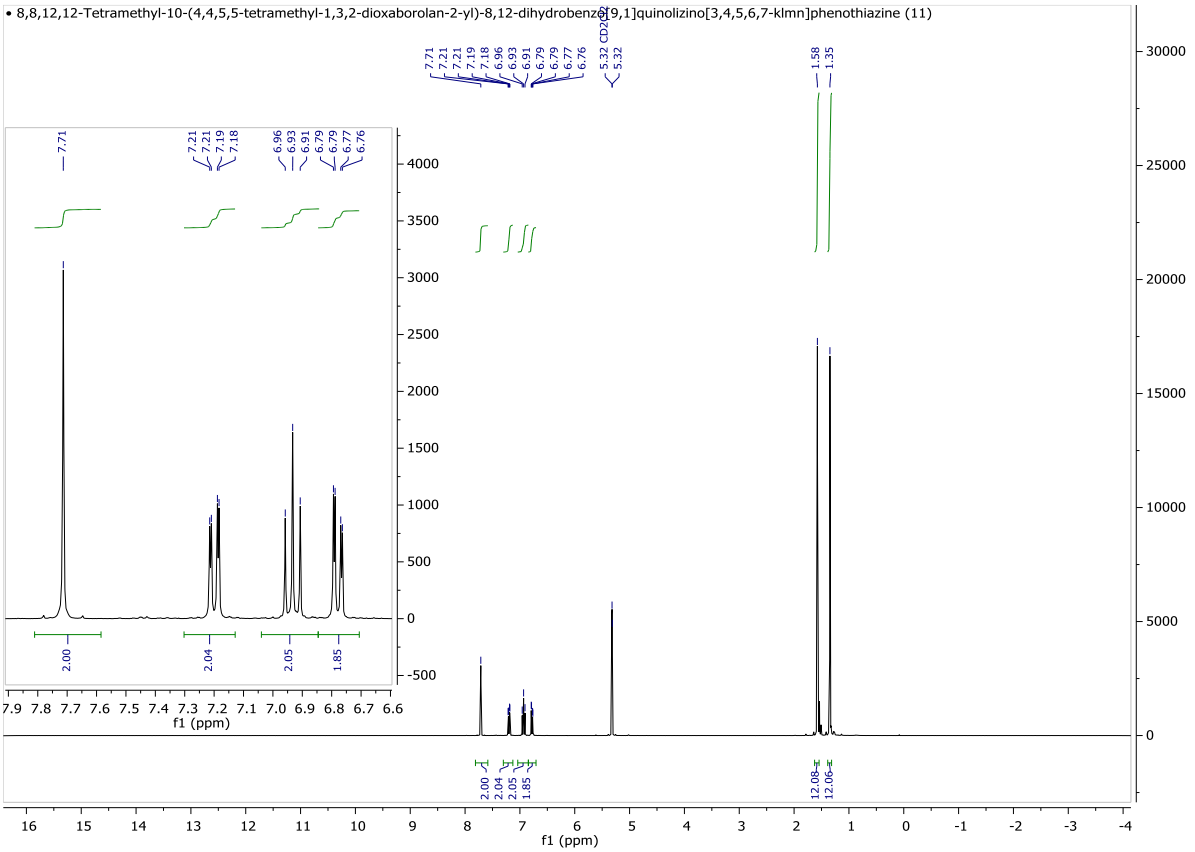

N,N′-Bis(2,6-diisopropyl-4-(8,8,12,12-tetramethyl-8,12-dihydrobenzo[9,1]quino-lizino-[3,4,5,6,7-klmn]phenothiazin-10-yl)phenyl)perylene-3,4:9,10-tetracarboxylic diimide (TT-Ph-PDI)

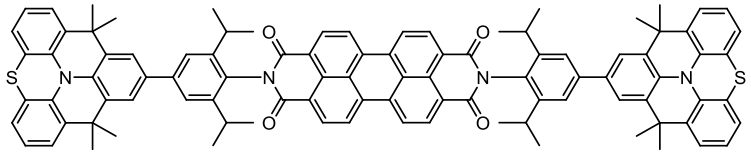

Mono-boronate *N*-heterotriangulene 11 (37 mg, 0.076 mmol), dibromo PDI 13 (30 mg, 0.035 mmol) and K_2CO_3 (95 mg, 0.691 mmol) were dissolved in a mixture of water (2 mL) and toluene (8 mL). The mixture was degassed by argon-bubbling for 30 minutes before $Pd(PPh_3)_4$ (4 mg, 0.1 eq.) was added. The reaction mixture was stirred at 85 °C for 8 hours under argon atmosphere.

The organic phase was separated and evaporated to dryness. The remaining solid was subjected to gel permeation chromatography (THF) and subsequently precipitated from methanol. The product was obtained as a dark red solid (24 mg, 49%).

^{1}H-NMR (500 MHz, THF-d_8) δ [ppm] = 9.06 (d, *J* = 8.2 Hz, 4H), 8.78 (d, *J* = 7.9 Hz, 4H), 7.67 (s, 4H), 7.53 (s, 4H), 7.29 (dd, *J* = 7.9, 1.7 Hz, 4H), 6.94 (t, *J* = 7.6 Hz, 4H), 6.80 (dd, *J* = 7.4, 1.6 Hz, 4H), 2.89 (p, *J* = 6.8 Hz, 4H), 1.69 (s, 24H), 1.24 (d, *J* = 6.8 Hz, 24H).

^{13}C-NMR (126 MHz, THF-d_8) δ [ppm] = 164.32, 147.31, 137.84, 136.25, 135.13, 132.69, 132.14, 131.52, 131.29, 131.14, 125.42, 125.33, 125.13, 125.01, 124.76, 123.63, 123.43, 117.43, 36.56, 33.26, 30.36, 24.47.

HR-MALDI TOF Ms (DCTB): *m/z* = 1416.5594; calc. for $C_{96}H_{80}N_4O_4S_2$ = 1416.5621.

FT-IR: $\tilde{\nu}$ [cm^{-1}] = 609, 728, 749, 758, 772, 788, 809, 839, 867, 964, 1033, 1062, 1123, 1179, 1197, 1213, 1253, 1301, 1343, 1404, 1429, 1463, 1579, 1595, 1663, 1700, 1740, 2849, 2917, 2956.

MP.: > 350 °C.

N,N′-Bis(2,6-diisopropyl-4-(4,4,5,5-tetramethyl-1,3,2-dioxaborolan-2-yl)phenyl)perylene-3,4:9,10-tetracarboxylic diimide (14)

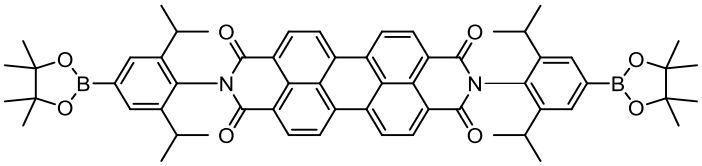

N,*N*′-Bis(4-bromo-2,6-di*iso*propylphenyl)perylene-3,4:9,10-tetracarboxylic diimide (13) (390 mg, 0.449 mmol), bis-pinacolato diboron (342 mg, 1.35 mmol) and potassium acetate (317 mg, 3.23 mmol) were dissolved in 1,4-dioxane (100 mL). Argon was bubbled through the solution for 30 minutes before $Pd(dppf)_2Cl_2$ (35 mg, 0.45 mmol) was added. The mixture was stirred at 85 °C under argon atmosphere for 5 hours. The organic solvent was removed under reduced pressure, then the remaining solid was dissolved in dichloromethane and filtered through a glass filter into petroleum ether (400 mL). The product was collected by filtration after the petroleum ether/dichloromethane solution had time to precipitate. Compound 14 was obtained as a dark red solid (42 %, 180 mg).

^{1}H-NMR (700 MHz, CD_2Cl_2) δ [ppm] = δ 8.78 (m, 8H), 7.77 (s, 4H), 2.77 (m, 4H), 1.39 (s, 24H), 1.18 (d, *J* = 6.6 Hz, 24H).

^{13}C-NMR (176 MHz, CD_2Cl_2) δ [ppm] = 164.07, 145.74, 135.73, 134.41, 132.45, 130.93, 130.75, 127.42, 124.12, 123.89, 84.53, 29.69, 25.23, 24.26.

FT-IR: $\tilde{\nu}$ [cm^{-1}] = 694, 746, 815, 852, 967, 1067, 1144, 1178, 1197, 1223, 1253, 1321, 1346, 1378, 1404, 1430, 1463, 1579, 1596, 1670, 1710, 2872, 2926, 2959.

MP.: > 350 °C.

HR MALDI-TOF MS (DCTB): m/z = 962.4147, calc. for $C_{60}H_{64}B_2N_2O_8$: 962.4849.

N,N′-Bis(4'-bromo-3,5-diisopropyl-2',5'-dioctyl-[1,1'-biphenyl]-4-yl)perylene-3,4:9,10-tetracarboxylic diimide (15)

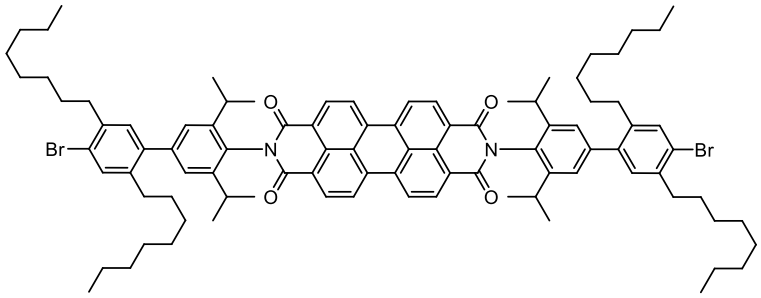

N,*N*′-Bis(2,6-di*iso*propyl-4-(4,4,5,5-tetramethyl-1,3,2-dioxaborolan-2-yl)phenyl)perylene-3,4:9,10-tetracarboxylic diimide (14) (100 mg, 0.104 mmol), 2,5-dibromo-1,4-dioctylbenzene (287 mg, 0.623 mmol) and K_2CO_3 (287 mg, 2.080 mmol) were dissolved in a mixture of toluene (40 mL) and water (5 mL). The mixture was degassed by argon-bubbling for 20 minutes before $Pd(PPh_3)_4$ (12 mg, 0.010 mmol) was added and the reaction mixture was stirred at 95 °C under argon atmosphere for 8 hours. The organic phase was extracted, evaporated to dryness and the crude product subjected to silica gel column chromatography (DCM:petroleum ether, 2:1). The product was obtained as bright red solid (124 mg, 81%).

^{1}H-NMR (500 MHz, CD_2Cl_2) δ [ppm] = 8.81 (s, 8H), 7.53 (s, 2H), 7.28 (s, 4H), 7.26 (s, 2H), 2.83 (q, *J* = 6.8 Hz, 4H), 2.80 – 2.74 (m, 4H), 2.67 – 2.59 (m, 4H), 1.67 (m, 4H), 1.64 (m, 4H), 1.48 – 1.23 (m, 48H), 1.19 (d, *J* = 6.8 Hz, 24H), 0.89 (m, 12H).

^{13}C-NMR (126 MHz, CD_2Cl_2) δ [ppm] = 164.19, 146.45, 142.54, 141.56, 140.59, 139.92, 135.74, 133.76, 132.47, 132.41, 130.78, 130.58, 127.46, 125.52, 124.13, 124.00, 123.83, 36.25, 33.26, 32.49, 32.45, 30.66, 30.24, 30.11, 30.04, 30.02, 29.88, 29.85, 29.80, 24.32, 23.28, 23.26, 14.47.

FD-MS (8kV): m/*z* = 1466.3 (100%) [M^+].

Elemental Analysis:

Calculated (%) C: 75.18, H: 7.68, N: 1.91;

Experimental (%) C: 74.83, H: 6.75, N: 2.02.

FT-IR: $\tilde{\nu}$ [cm^{-1}] = 751, 802, 810, 964, 1020, 1051, 1081, 1094, 1178, 1198, 1256, 1344, 1379, 1404, 1453, 1467, 1579, 1595, 1673, 1708, 2854, 2924, 2953.

MP.: 248 °C.

N,N′-Bis(3,5-diisopropyl-2',5'-dioctyl-4'-(4,4,5,5-tetramethyl-1,3,2-dioxaborolan-2-yl)-[1,1'-biphenyl]-4-yl)perylene-3,4:9,10-tetracarboxylic diimide (16)

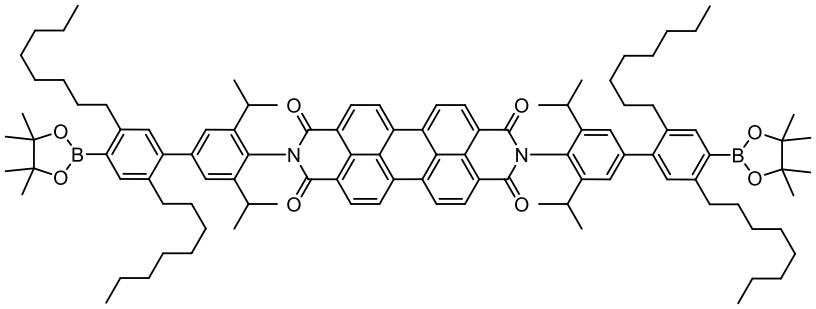

N,*N*′-Bis(4'-bromo-3,5-di*iso*propyl-2',5'-dioctyl-[1,1'-biphenyl]-4-yl)perylene-3,4:9,10-tetracarboxylic diimide (15) (100 mg, 0.068 mmol), bis-pinacolato diboron (86 mg, 0.340 mmol) and potassium acetate (48 mg, 0.490 mmol) were dissolved in 1,4-dioxane (50 mL). Argon was bubbled through the solution for 30 minutes before $Pd(dppf)_2Cl_2$ (5 mg, 0.007 mmol) was added. The mixture was stirred at 85 °C under argon atmosphere overnight. The organic solvent was removed, the residue then subjected to flash silica gel column chromatography (DCM/PE, 1:2). The product was obtained as dark red solid (72 mg, 68%).

^{1}H-NMR (500 MHz, CD_2Cl_2) δ [ppm] = 8.81 (s, 8H), 7.71 (s, 2H), 7.31 (s, 4H), 7.21 (s, 2H), 2.94 – 2.88 (m, 4H), 2.82 (p, *J* = 6.8 Hz, 4H), 2.70 – 2.62 (m, 4H), 1.68 – 1.56 (m, 8H), 1.46 – 1.21 (m, 40H), 1.38 (s, 24H), 1.19 (d, *J* = 6.8 Hz, 24H), 0.89 (td, *J* = 6.9, 3.1 Hz, 12H).

^{13}C-NMR (126 MHz, CD_2Cl_2) δ [ppm] = 164.23, 148.17, 146.26, 144.49, 143.55, 137.85, 137.30, 135.74, 132.47, 131.51, 130.80, 130.38, 127.48, 125.52, 124.13, 124.06, 83.98, 36.02, 34.24, 33.47, 33.06, 32.56, 32.49, 30.54, 30.46, 30.29, 30.20, 30.18, 30.00, 29.94, 29.83, 24.36, 23.31, 23.28, 14.49, 1.36.

FT-IR: $\tilde{\nu}$ [cm^{-1}] = 749, 812, 851, 1024, 1067, 1130, 1147, 1177, 1197, 1254, 1347, 1354, 1404, 1430, 1464, 1579, 1596, 1667, 1708, 2854, 2926, 2959.

MP.: > 250 °C.

HR MALDI-TOF MS (DCTB): m/*z* = 1563.0609, calc. for $C_{104}H_{136}B_2N_2O_8$: 1563.0483.

N,N′-Bis(4'-(4,4,8,8,12,12-hexamethyl-6,10-bis(4-(methylthio)phenyl)-8,12-dihy-dro-4H-benzo[9,1]quinolizino[3,4,5,6,7-defg]acridin-2-yl)-3,5-diisopropyl-2',5'-dioctyl-[1,1'-biphenyl]-4-yl)perylene-3,4:9,10-tetracarboxylic diimide (T-(Ph)$_2$-PDI)

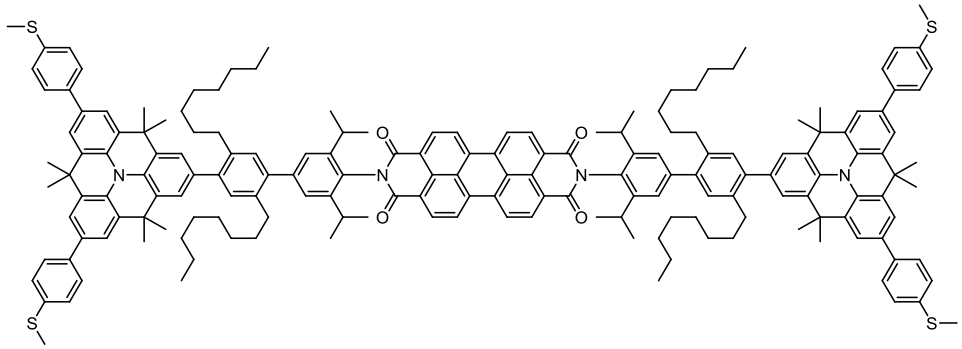

N,*N*′-Bis(3,5-di*iso*propyl-2',5'-dioctyl-4'-(4,4,5,5-tetramethyl-1,3,2-dioxaborolan-2-yl)-[1,1'-biphenyl]-4-yl)perylene-3,4:9,10-tetracarboxylic diimide (16) (31 mg, 0.020 mmol) and 2-bromo-4,4,8,8,12,12-hexamethyl-6,10-bis(4-(methylthio)phenyl)-8,12-dihydro-4*H*-benzo[9,1]quinolizino[3,4,5,6,7-*defg*]acridine (4) (30 mg, 0.044 mmol) were dissolved in toluene (5 mL). K_2CO_3 (82 mg, 0.594 mmol), a tiny amount of 18-crown-6 and a drop of *Aliquat 336* were added together with water (2 mL). The mixture was degassed by argon-bubbling for 30 minutes before $Pd(PPh_3)_4$ (2 mg, 0.1 eq.) was added. The reaction mixture was stirred at 85 °C for 2 hours under argon atmosphere. The organic phase was separated and evaporated to dryness. The remaining solid was subjected to gel permeation chromatography (THF) to separate the product from remaining uncoupled *N*-heterotriangulene byproducts. The red fractions were combined and subsequently purified via silica gel column chromatography (very short, DCM/PE, 1:1) under the exclusion of light. The product was obtained as dark red solid (30 mg, 60%).

^{1}H-NMR (300 MHz, CD_2Cl_2) δ [ppm] = 8.83 (s, 8H), 7.69 (s, 8H), 7.66 (d, *J* = 8.4 Hz, 8H), 7.50 (s, 4H), 7.44 – 7.34 (m, 16H), 2.87 (q, *J* = 6.8 Hz, 4H), 2.81 – 2.68 (m, 8H), 2.56 (s, 12H), 1.80 (m, 36H), 1.38 – 1.15 (m, 72H), 0.94 – 0.86 (m, 12H).

^{13}C-NMR (75 MHz, CD_2Cl_2) δ [ppm] = 164.27, 146.36, 143.45, 141.63, 141.16, 138.71, 138.40, 138.37, 137.75, 137.02, 135.75, 135.30, 132.51, 131.75, 131.06, 130.97, 130.85, 130.81, 130.40, 130.26, 127.56, 127.43, 125.99, 125.74, 125.44, 124.15, 124.06, 122.72, 122.56, 53.64, 36.51, 36.41, 34.70, 33.96, 33.73, 32.50, 32.45, 30.70, 30.51, 30.38, 30.29, 30.21, 30.01, 29.94, 29.80, 24.43, 23.29, 23.21, 16.38, 14.43.

HR-MALDI TOF Ms (DCTB): *m/z* = 2525.3481; calc. for $C_{174}H_{188}N_4O_4S_4$ = 2525.3513.

FT-IR: $\tilde{\nu}$ [cm^{-1}] = 749, 768, 809, 851, 859, 882, 955, 969, 1014, 1070, 1098, 1122, 1158, 1179, 1197, 1209, 1252, 1287, 1303, 1317, 1341, 1354, 1381, 1403, 1444, 1466, 1579, 1596, 1669, 1705, 2854, 2924, 2957.

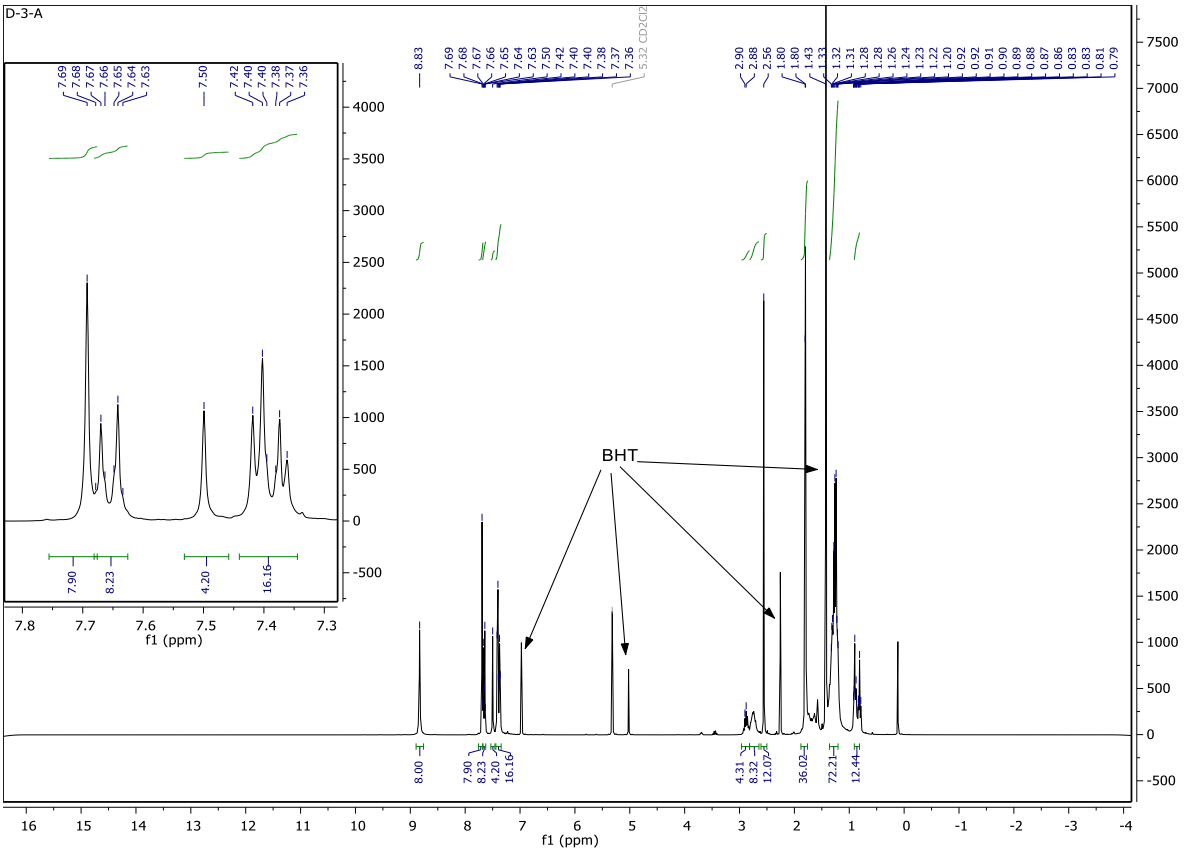

N,N′-Bis(4'''-(4,4,8,8,12,12-hexamethyl-6,10-bis(4-(methylthio)phenyl)-8,12-dihydro-4H-benzo[9,1]quinolizino[3,4,5,6,7-defg]acridin-2-yl)-3,5-diisopropyl-2'',5''-dioctyl-[1,1':4',1'':4'',1'''-quaterphenyl]-4-yl)perylene-3,4:9,10-tetracarboxylic diimide (T-(Ph)$_4$-PDI)

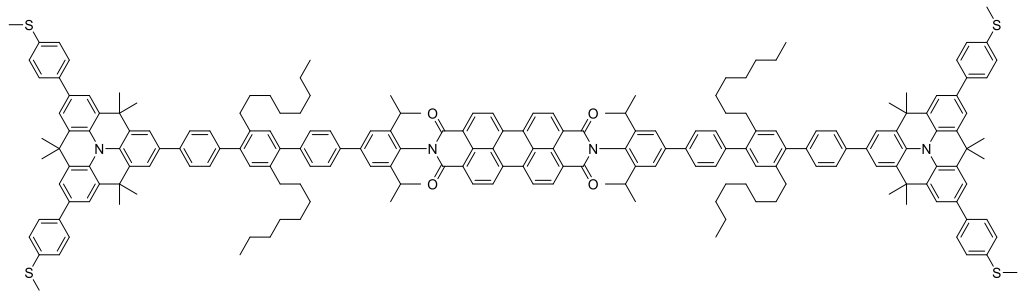

2-Bromo-4,4,8,8,12,12-hexamethyl-6,10-bis(4-(methylthio)phenyl)-8,12-dihydro-4*H*-benzo[9,1]quinolizino[3,4,5,6,7-*defg*]acridine (4) (30 mg, 0.044 mmol) and bis-boronate PDI 17 (37 mg, 0.020 mmol) were dissolved in toluene (5 mL). K_2CO_3 (82 mg, 0.594 mmol), a tiny amount of 18-crown-6 and a drop of *Aliquat 336* were added together with water (2 mL). The mixture was degassed by argon-bubbling for 30 minutes before $Pd(PPh_3)_4$ (2 mg, 0.1 eq.) was added. The reaction mixture was stirred at 85

°C under argon atmosphere overnight. The organic phase was separated and evaporated to dryness. The remaining solid was subjected to gel permeation chromatography (THF). The first fraction was then subjected to alox column chromatography (very short, DCM/PE, 1:1 to 1:0) under the exclusion of light. The product was obtained as a dark red solid (80 mg, 14%).

^{1}H-NMR (300 MHz, CD_2Cl_2) δ [ppm] = 8.84 (s, 8H), 7.85 – 7.75 (m, 14H), 7.67 (dq, *J* = 4.3, 2.1 Hz, 18H), 7.63 (s, 4H), 7.53 (t, *J* = 8.5 Hz, 10H), 7.43 – 7.34 (m, 9H), 7.26 (d, *J* = 3.1 Hz, 5H), 2.87 (p, *J* = 6.8 Hz, 4H), 2.69 (d, *J* = 8.2 Hz, 9H), 2.55 (s, 14H), 1.81 (s, 33H), 1.78 (s, 15H), 1.61 (d, *J* = 8.1 Hz, 9H), 1.26 (d, *J* = 7.1 Hz, 88H), 0.93 – 0.80 (m, 17H).

^{13}C-NMR (75 MHz, CD_2Cl_2) δ [ppm] = 164.29, 147.12, 142.76, 141.91, 141.16, 140.97, 140.18, 139.87, 138.29, 137.75, 136.36, 135.78, 135.36, 132.55, 131.65, 131.55, 131.04, 131.01, 130.80, 130.36, 127.66, 127.46, 127.44, 127.41, 126.69, 125.96, 124.17, 123.95, 123.69, 122.90, 122.66, 36.48, 34.66, 33.82, 33.78, 33.21, 32.44, 32.16, 30.64, 30.11, 29.88, 29.76, 24.37, 23.25, 21.39, 16.31, 14.46.

HR-MALDI TOF Ms (DCTB): *m/z* = 2829.4758; calc. for $C_{198}H_{204}N_4O_4S_4$ = 2829.4765.

FT-IR: $\tilde{\nu}$ [cm^{-1}] = 738, 749, 768, 812, 818, 838, 859, 885, 897, 958, 968, 1014, 1058, 1097, 1124, 1151, 1181, 1198, 1213, 1254, 1288, 1303, 1319, 1341, 1356, 1404, 1443, 1580, 1596, 1667, 1703, 2854, 2924, 2957.

Supplementary Note 2. CYCLIC VOLTAMMETRY

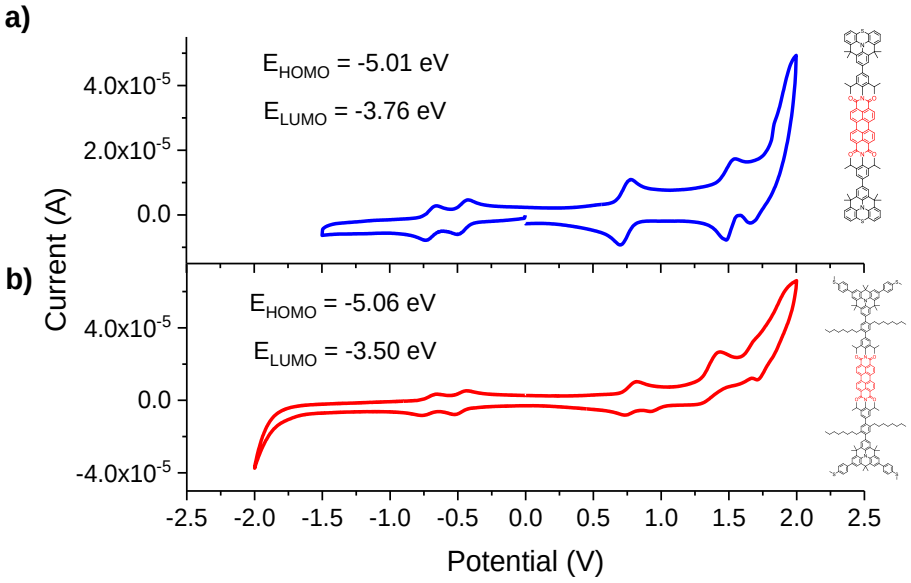

Figure S 1 Cyclic voltammetrey of (a) **TT-Ph-PDI**, (b) **T-(Ph)$_2$-PDI**. Potential vs. Fc/Fc$^+$.

Supplementary Note 3. UV-VIS SPECTRUM

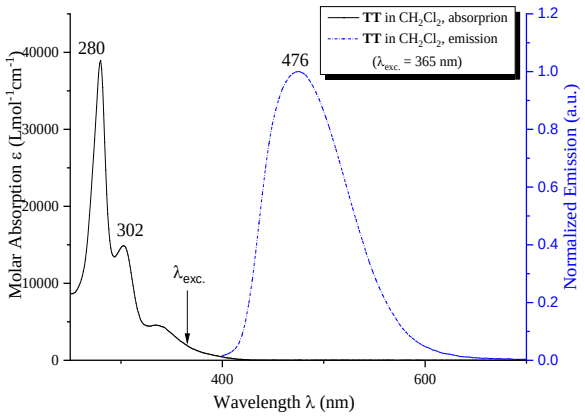

Figure S 2 UV/Vis spectrum of **Thiotriangulene** in solution (dichloromethane). Solid black graph shows the absorption, dashed blue graph the emission spectrum.

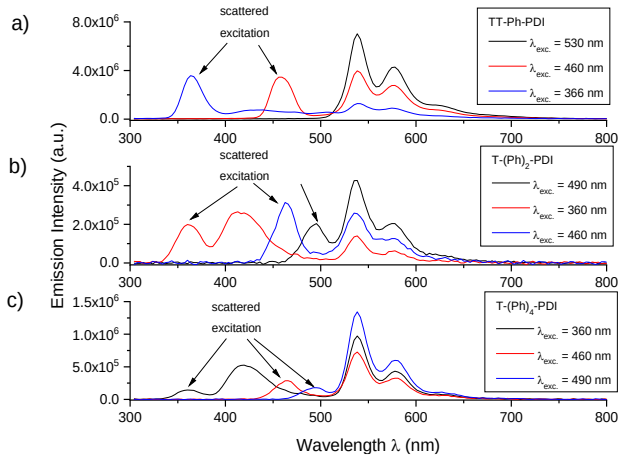

Figure S 3 Photoluminescence spectra of a) TT-Ph-PDI, b) T-$(Ph)_2$-PDI, and c) T-$(Ph)_4$-PDI in solution (dichloromethane). Spectra were recorded at different excitation wavelengths.

Supplementary Note 4. TD-DFT OF EXCITED STATES

Ground state geometries were optimized using the m062x range-separated functional and the 6-311g(d) basis set. All optimizations were performed in the implicit solvent (dichloromethane) using the IEFPCM model. Absorption spectra were calculated at the same level of theory using non-equilibrium solvation model (PISALR) in which only the electronic relaxation is taken into account. All calculations were performed using the GAUSSIAN 09 package.

The first 10 calculated excited states (ordering corresponds to the gas phase calculations) have distinct features either of an excited PDI moiety (states 1 and 6), CT states (2, 3, 7, 8) or trianguline (states 4 and 5). Adding non-equilibrium (electronic only) stabilization of the excited state leads to the re-ordering of the states, in particular the doubly degenerate CT state becomes the lowest excited state, followed by the first excited state of PDI. This implies that the trianguline is a relatively weak with respect to PDI donor, with the energy offset of ca 0.4 eV. To illustrate the character of the transition, the natural transition orbitals are shown in Figure S , together with excited state energies and oscillator strengths.

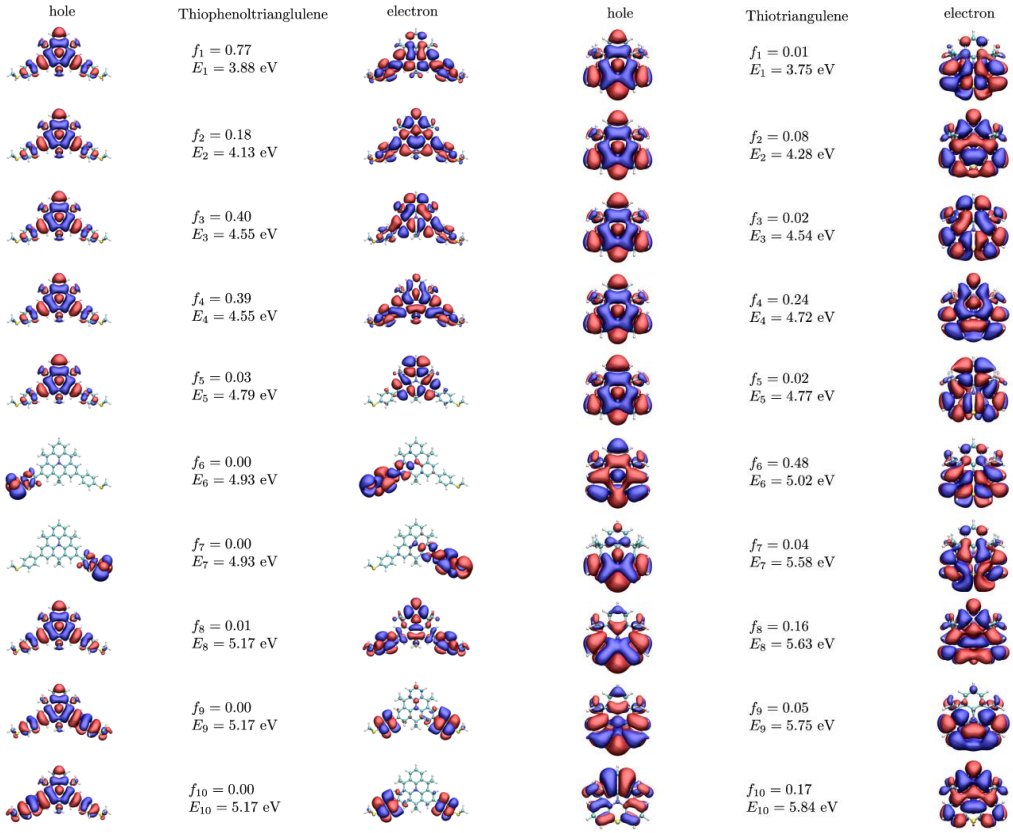
hole
Thiophenoltrianglulene
electron
hole
Thiotriangulene
electron
$f_1 = 0.77$
$E_1 = 3.88$ eV
$f_2 = 0.18$
$E_2 = 4.13$ eV
$f_3 = 0.40$
$E_3 = 4.55$ eV
$f_4 = 0.39$
$E_4 = 4.55$ eV
$f_5 = 0.03$
$E_5 = 4.79$ eV
$f_6 = 0.00$
$E_6 = 4.93$ eV
$f_7 = 0.00$
$E_7 = 4.93$ eV
$f_8 = 0.01$
$E_8 = 5.17$ eV
$f_9 = 0.00$
$E_9 = 5.17$ eV
$f_{10} = 0.00$
$E_{10} = 5.17$ eV
$f_1 = 0.01$
$E_1 = 3.75$ eV
$f_2 = 0.08$
$E_2 = 4.28$ eV
$f_3 = 0.02$
$E_3 = 4.54$ eV
$f_4 = 0.24$
$E_4 = 4.72$ eV
$f_5 = 0.02$
$E_5 = 4.77$ eV
$f_6 = 0.48$
$E_6 = 5.02$ eV
$f_7 = 0.04$
$E_7 = 5.58$ eV
$f_8 = 0.16$
$E_8 = 5.63$ eV
$f_9 = 0.05$
$E_9 = 5.75$ eV
$f_{10} = 0.17$
$E_{10} = 5.84$ eV

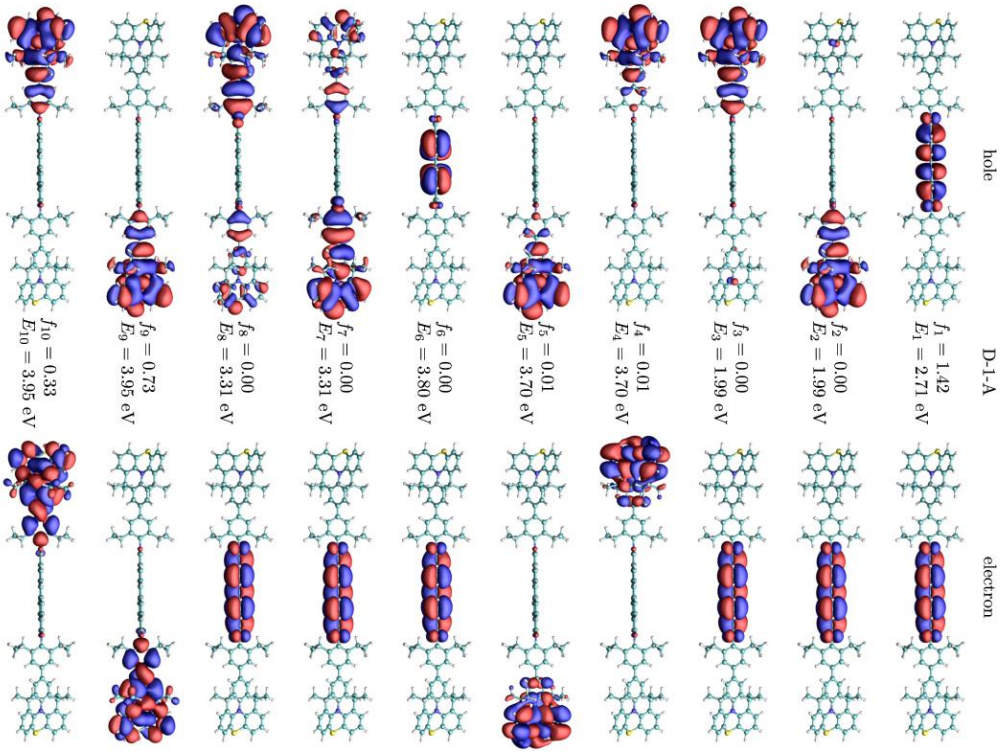
hole
D-1-A
electron
$f_1 = 1.42$
$E_1 = 2.71$ eV
$f_2 = 0.00$
$E_2 = 1.99$ eV
$f_3 = 0.00$
$E_3 = 1.99$ eV
$f_4 = 0.01$
$E_4 = 3.70$ eV
$f_5 = 0.01$
$E_5 = 3.70$ eV
$f_6 = 0.00$
$E_6 = 3.80$ eV
$f_7 = 0.00$
$E_7 = 3.31$ eV
$f_8 = 0.00$
$E_8 = 3.31$ eV
$f_9 = 0.73$
$E_9 = 3.95$ eV
$f_{10} = 0.33$
$E_{10} = 3.95$ eV

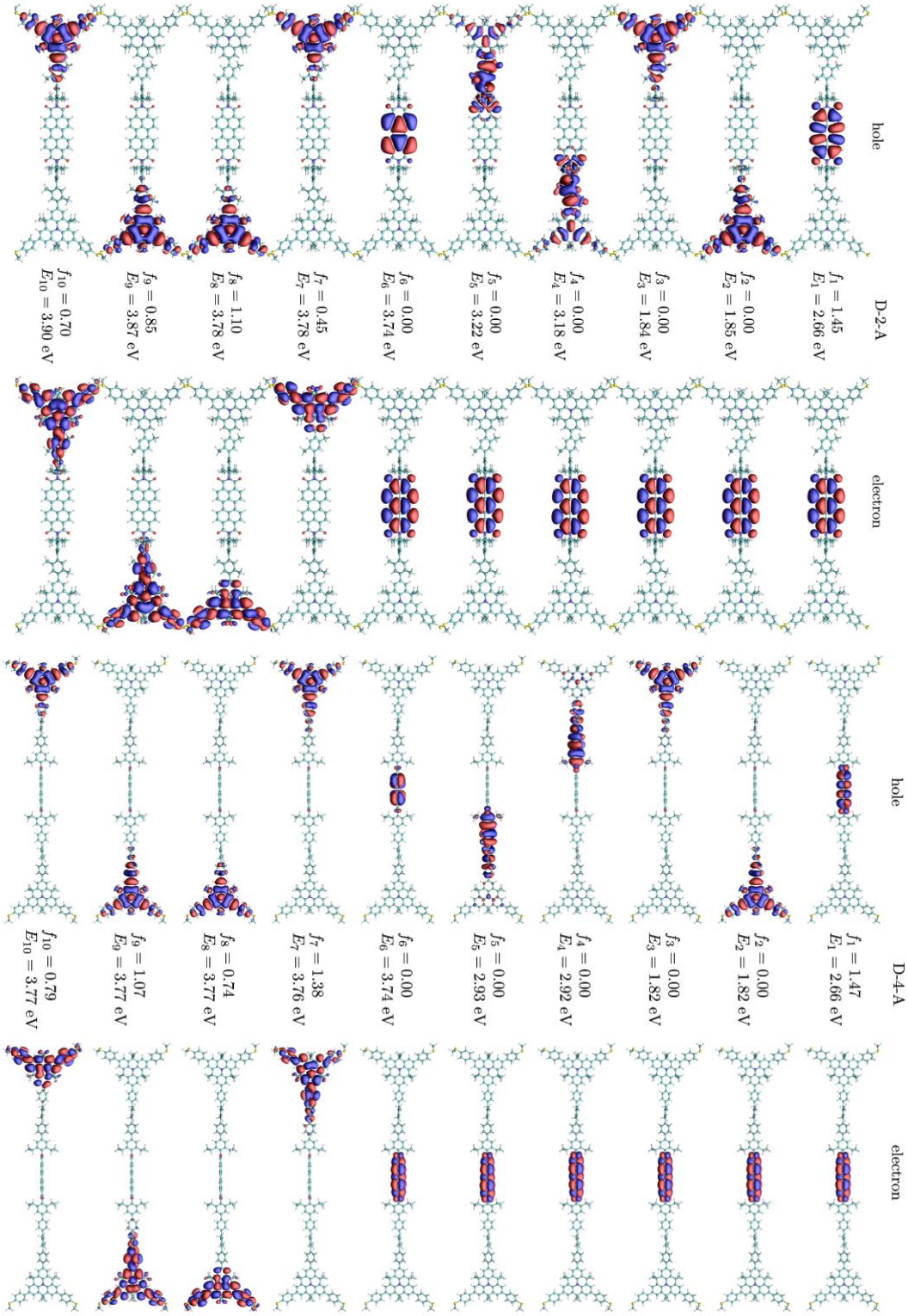

Figure S 4 *Natural transition orbitals of the first ten excited states of thiophenoltriangulene, thiotriangulene, TT-Ph-PDI, T-(Ph)$_2$-PDI, and T-(Ph)$_4$-PDI calculated at the m062x/6-31g(d) level of theory.*

Supplementary Note 5. EXTINCTION COEFFICIENT

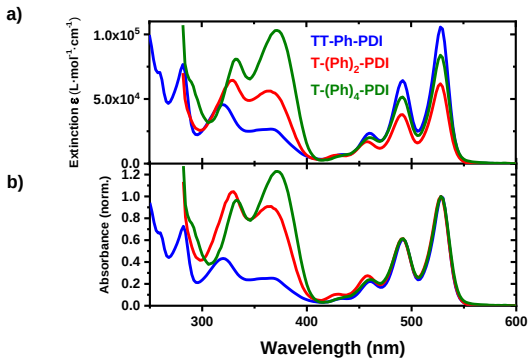

Figure S 5 (a) Extinction coefficient and (b) normalized UV-Vis absorption spectra of dilute solution of the three dyads, **TT-Ph-PDI** (blue), **T-(Ph)$_2$-PDI** (red), and **T-(Ph)$_4$-PDI** (green).

Supplementary Note 6. PHOTO-INDUCED ABSORPTION

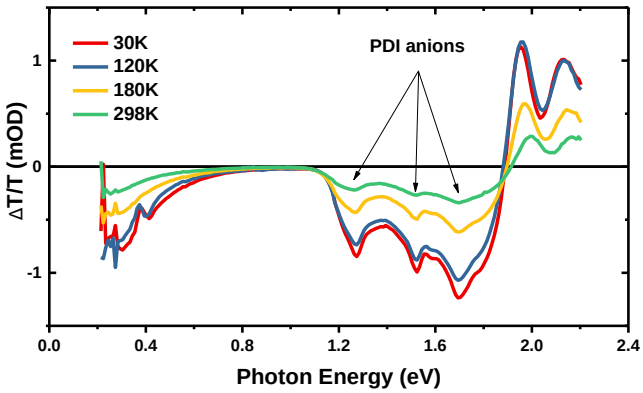

Figure S 6 Photo-induced absorption (PIA) spectra of P3HT:PDI blend 3:1 at various temperatures photo-excited with 514nm laser at 30 mW.

The spectrum of PDI anions (superposed with P3HT cations) obtained by electron transfer from photoexcited P3HT and measured by photo induced absorption (PIA) spectroscopy.

Supplementary Note 7. MULTIVARIATE CURVE RESOLUTION ALTERNATING LEAST SQUARES ANALYSIS (MCR-ALS)

Singular value decomposition (SVD) applied to TA datasets of **TT-Ph-PDI** upon acceptor excitation (D-S-A*) estimates that the contributions from two components is sufficient to describe the TA dataset. Subsequent MCR-ALS analysis with non-negativity of kinetics as the only constraint,[1] is shown in Figure S7. The component spectra obtained by MCR analysis (Figure S 7b) have distinct features that aid their identification. The first component (dark blue line) is assigned to PDI excitons, since it exhibits a clear GSB and SE, resembling the absorption and emission of PDI molecules including their vibronic transitions. The second component (light blue line) exhibits the typical GSB and ESA features of PDI anions, hence, it is assigned to intramolecular CT-states.

We now turn to the dynamics of excitons and intramolecular CT-states, shown in Figure S7c. The fast decay of excitons (dark blue spheres) is accompanied by a fast rise of the population of intramolecular CT-states (light blue spheres) with some charges being already generated within the time resolution of our fast TA setup. The population of intramolecular CT states reaches a maximum at around 5 ps, and subsequently the CT states recombine with a significantly smaller decay rate compared to their generation.

Applying the MCR analysis to the TA data of **T-(Ph)$_2$-PDI** and **T-(Ph)$_4$-PDI**, we obtained their component-associated spectra and dynamics (see Figures S8 and Figure S9). MCR identified the same two component spectra as for **TT-Ph-PDI**, that is, PDI excitons and intramolecular CT-states, but with dynamics clearly slowing down with increasing the spacer length. From molecule **TT-Ph-PDI** to **T-(Ph)$_2$-PDI** and **T-(Ph)$_4$-PDI**: both exciton decay and charge generation slow down. Similarly, intramolecular CT-states live considerably longer, up to hundreds of nanoseconds in case of **T-(Ph)$_4$-PDI**.

The CT states in **T-(Ph)$_4$-PDI** decay to 50% of the initial population within 8 ns, which is the maximum time-delay of our TA setup. We also performed TA measurements in the ns-µs time range to obtain the lifetimes of CT states. The measurements were performed by electronically delaying a 532 nm pump laser (see Figure S10).

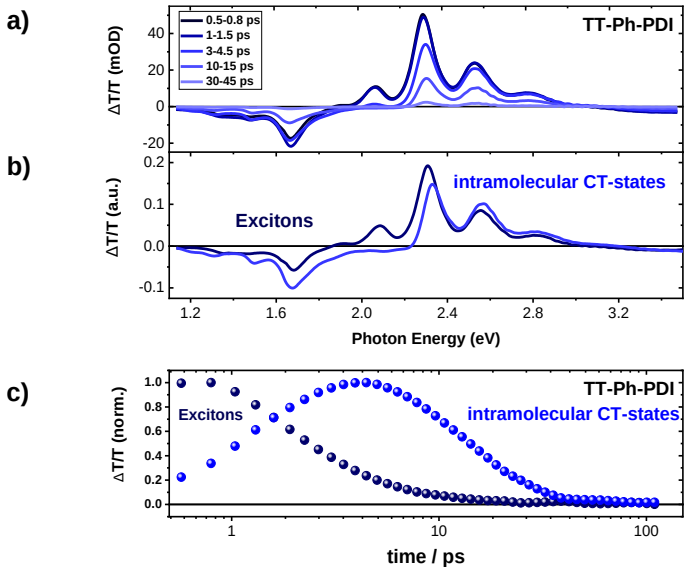

Figure S 7 (a) TA spectra of **TT-Ph-PDI** molecule in diluted solution. (b) PDI exciton spectrum (dark blue) and intramolecular CT-states spectrum (light blue) as obtained by MCR analysis. (c) Dynamics of the MCR obtained PDI excitons (dark blue spheres) and intramolecular CT-states (light blue spheres).

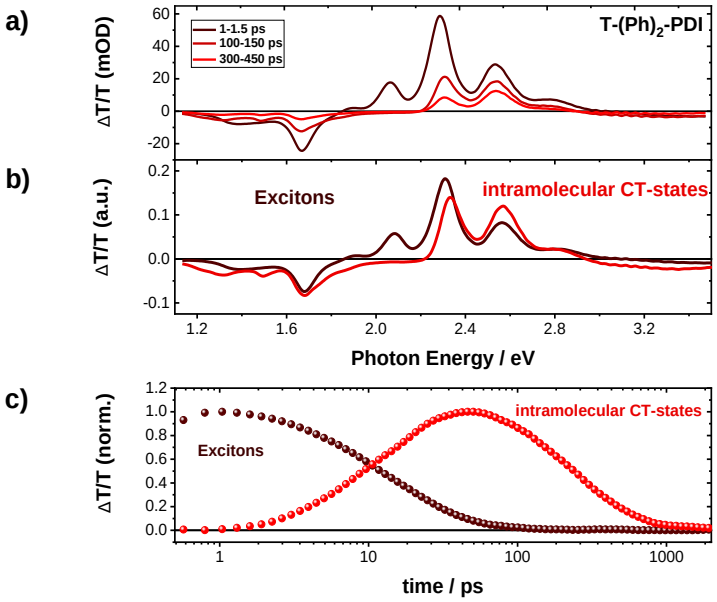

Figure S 8 (a) Transient absorption (TA) spectra of **T-(Ph)$_2$-PDI** in solution photo-excited at 490 nm (excitation density 53 µJ/cm^2). (b) PDI exciton spectrum (dark red) and intramolecular CT-states spectrum (light red) as obtained by MCR analysis. (c) Dynamics of the MCR obtained PDI excitons (dark red spheres) and intramolecular CT-states (light red spheres).

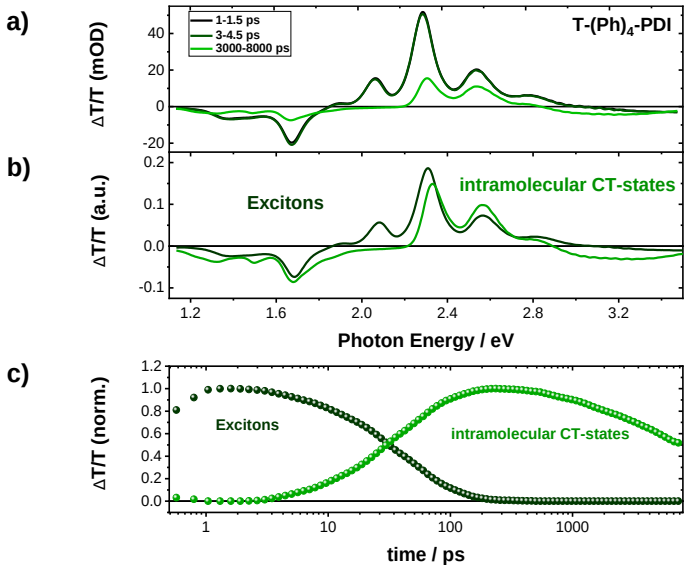

Figure S 9 (a) Transient absorption (TA) spectra of **T-(Ph)$_4$-PDI** in solution photo-excited at 490 nm (excitation density 53 µJ/cm^2). (b) PDI exciton spectrum (dark green) and intramolecular CT-states spectrum (light green) as obtained by MCR analysis. (c) Dynamics of the MCR obtained PDI excitons (dark green spheres) and intramolecular CT-states (light green spheres).

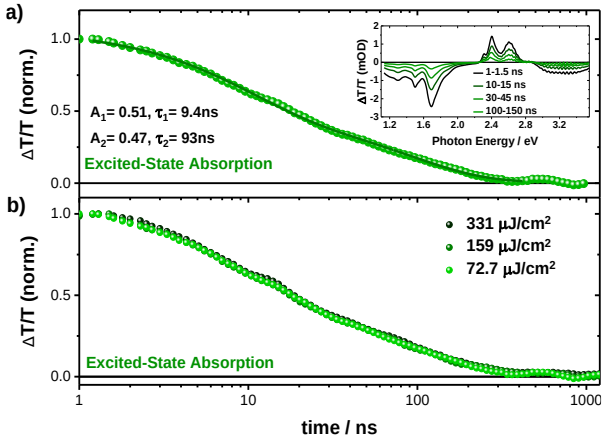

Figure S 10 (a) Excited-state absorption decay dynamics of **T-(Ph)$_4$-PDI** in dilute solution excited at 532nm (excitation density 72.7 µJ/cm^2) fitted by a bi-exponential function (solid line). Inset: transient absorption (TA) spectra at different time delays. (b) Excited-state absorption dynamic at various excitation densities.

Supplementary Note 8. TA SPECTRA FOLLOWING THE DONOR EXCITATION

Figure S 11a shows the TA spectra of **T-(Ph)$_2$-PDI** at different time delays. The spectrum at early time delays (0.5-0.8 ps) reveals a broad ESA throughout the entire range of probe energies. We assign this broad feature to the triangulene donor since the 355 nm excited state transition of triangulene is optically active,

as confirmed by previous excited state calculation. While the ESA decays, the generation of PDI excitons and anions is observed. This is apparent from spectra recorded at later time delays and it is a clear indication of energy transfer from the excited donor to the PDI core.[2] To resolve the different processes following excitation of the donor, we again used MCR analysis. Figure S 11b clearly shows the spectral contribution of the triangulene exciton as a broad ESA feature, while the other two states observed are PDI excitons and intramolecular CT-states as discussed above. The dynamics of these states (see Figure S 11c) hints to parallel and competing processes of energy transfer from the triangulene to PDI and direct electron transfer from triangulene. This could be deduced from the population dynamics of intramolecular CT-states and PDI excitons at 2 ps, showing that 20% of CT-states are being generated significantly faster than the PDI excitons. However, this initial rise of CT-states population is around the temporal resolution of our TA setup and could be due to the laser pulse excitation. Meanwhile, energy transfer takes place and populates PDI excitons followed by consecutive forward hole transfer process populating also the intramolecular CT-states.

Similarly, these processes occur in the **T-(Ph)$_4$-PDI** dyads when exciting the triangulene (see Figure S12). However, energy transfer from triangulene to PDI excitons is slower in **T-(Ph)$_4$-PDI** and followed by slower hole transfer compared to **T-(Ph)$_2$-PDI**. Excitation of thiotriangulene in the **TT-Ph-PDI** dyad, on the other hand, results in energy transfer faster than the temporal resolution of our TA setup (Figure S13).

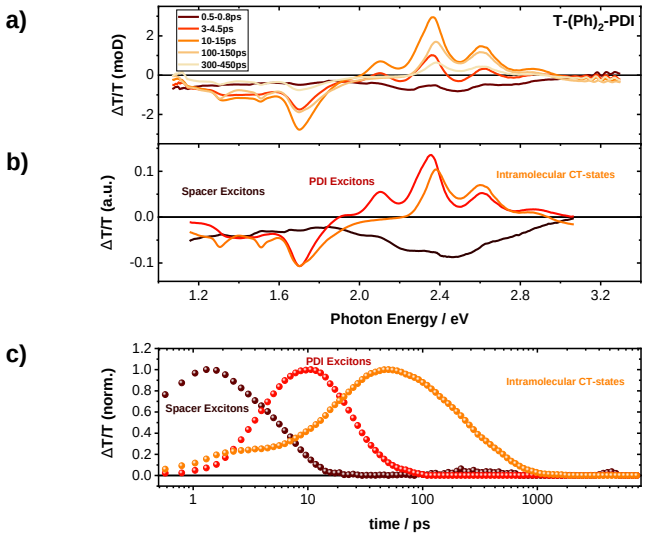

Figure S 11 (a) Transient absorption (TA) spectra of **T-(Ph)$_2$-PDI** in solution photo-excited at 355 nm (excitation density 86 µJ/cm^2). (b) Triangulene excitons (brown line), PDI exciton spectrum (red line) and intramolecular CT-states spectrum (orange line) as obtained by MCR analysis. (c) Dynamics of the MCR obtained triangulene excitons (brown spheres), PDI excitons (red spheres) and intramolecular CT-states (orange spheres).

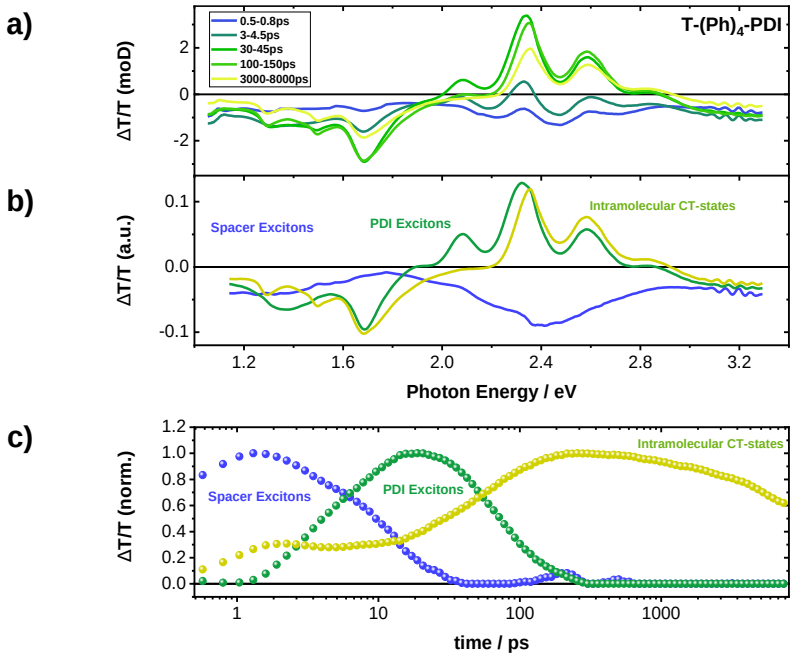

Figure S 12 (a) Transient absorption (TA) spectra of **T-(Ph)$_4$-PDI** in solution photo-excited at 355 nm (excitation density 81 µJ/cm^2). (b) Triangulene excitons (blue line), PDI exciton spectrum (green line) and intramolecular CT-states spectrum (yellow line) as obtained by MCR analysis. (c) Dynamics of the MCR obtained triangulene excitons (blue spheres), PDI excitons (green spheres) and intramolecular CT-states (yellow spheres).

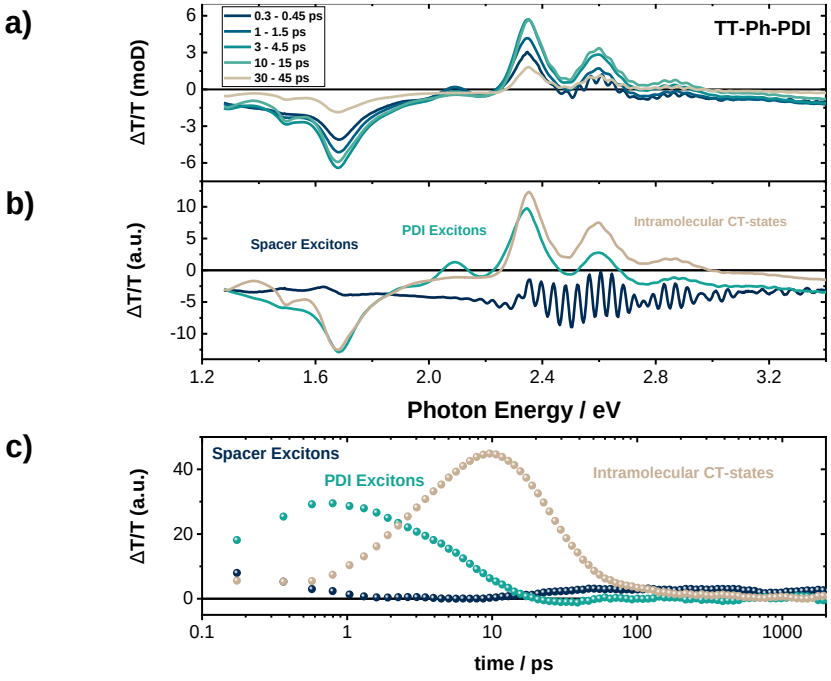

Figure S 13 (a) Transient absorption (TA) spectra of **TT-Ph-PDI** in solution photo-excited at 355 nm (excitation density 62 µJ/cm^2). (b) Thiotriangulene excitons (dark blue line), PDI exciton spectrum (light blue line) and intramolecular CT-states spectrum (beige line) as obtained by MCR analysis. (c) Dynamics of the MCR obtained thiotriangulene excitons (dark blue spheres), PDI excitons (light blue spheres) and intramolecular CT-states (beige spheres).

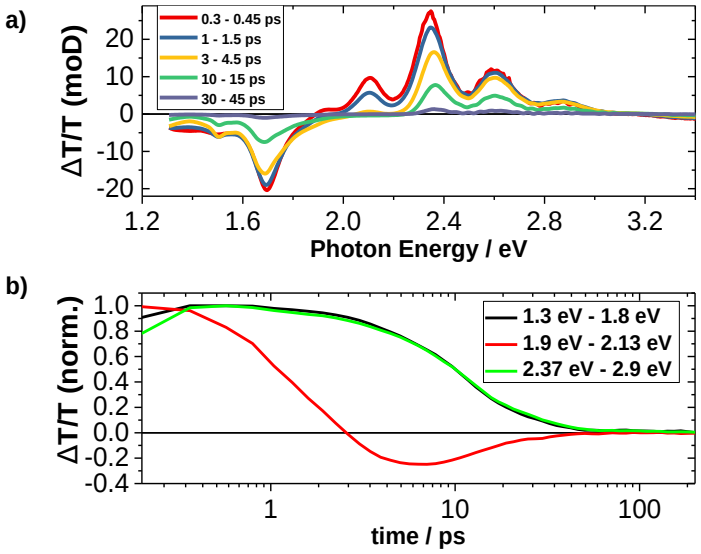

Figure S 14 (a) Transient absorption (TA) spectra of **TT-Ph-PDI** in solution photo-excited at 490 nm (excitation density 19.1 µJ/cm^2). (b) Dynamics extracted between 1.3-1.8 eV (black line), 1.9-2.13 eV (red line) and 2.37-2.9 eV (green line).

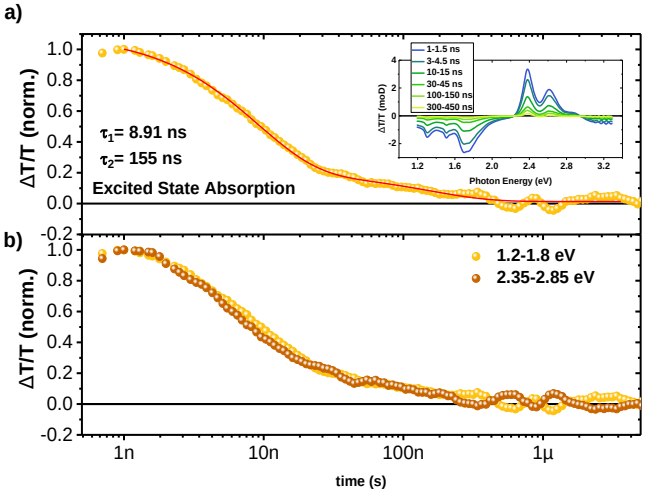

Figure S 15 (a) Excited-state absorption decay dynamics of **T-(Ph)4-PDI** in dilute solution excited at 355 nm (excitation density 79 µJ/cm^2) fitted by a bi-exponential function (solid line). Inset: transient absorption (TA) spectra at different time delays. (b) Dynamic of excited-state absorption (1.2-1.8 eV) and ground-state bleach (2.35-2.85 eV).

Supplementary Note 9. SOLUTION OF RATE EQUATIONS

To fit the MCR output dynamics and extract the rates of energy transfer, hole transfer and charge recombination, we solved the rate equations presented in Figure 5. The solution for acceptor excitation D-S-A* reads:

$$[\mathrm{a}^*] = A_0 e^{-(t-t_0)k_{\mathrm{a}^*\rightarrow\mathrm{ct}}}$$

$$[\mathrm{ct}] = A_1 e^{-(t-t_0)k_{\mathrm{a}^*\to\mathrm{ct}}} + A_2 e^{-(t-t_0)k_{\mathrm{ct}\to\mathrm{g}}}$$

while the solution for donor excitation D*-S-A is shown below:

$$[\mathrm{d}^*] = A_0 e^{-(t-t_0)(k_{\mathrm{d}^*\to\mathrm{a}^*}+k_{\mathrm{d}^*\to\mathrm{ct}})}$$

$$[\mathrm{a}^*] = A_1 e^{-(t-t_0)k_{\mathrm{a}^*\to\mathrm{ct}}} - A_2 e^{-(t-t_0)(k_{\mathrm{d}^*\to\mathrm{a}^*}+k_{\mathrm{d}^*\to\mathrm{ct}})}$$

$$[\mathrm{ct}] = A_3 e^{-(t-t_0)k_{\mathrm{ct}\to\mathrm{g}}} - A_4 e^{-(t-t_0)k_{\mathrm{a}^*\to\mathrm{ct}}} - A_5 e^{-(t-t_0)(k_{\mathrm{d}^*\to\mathrm{a}^*}+k_{\mathrm{d}^*\to\mathrm{ct}})}$$

The global fit in Figure 6 for donor excitation D*-S-A showed negligible values for direct electron transfer from triangulene to CT-states ($k_{\mathrm{d}^*\to\mathrm{ct}}$). For this reason, this rate was excluded from the fit and was not shown in the set of rate equations in Figure 5.

Supplementary Note 10. DRIVING FORCES AND REORGANIZATION ENERGIES

We are interested in two charge transfer rates: excited PDI to the charge transfer state, $k^{\mathrm{a}^*\to\mathrm{ct}}$, and CT to the ground state, $k^{\mathrm{ct}\to\mathrm{g}}$. Hence, four electronic states are of a particular interest: the excited donor state, D*-A-D; the charge transfer state, D^+- A^--D (which can also be of a quadrupolar type, D^+-A^--D^+); the excited acceptor state (PDI), D-A*-D; and the ground state, D-A-D. We refer to these states as d*, ct, a*, and g, respectively. The corresponding equilibrium geometries of the molecular and solvent coordinates are denoted by the capital letters, that is, D*, CT, A*, and G. As an illustration, the energy of a charge transfer state in a ground state geometry is $E_{\mathrm{ct}}^{\mathrm{G}}$. We also introduce four vertical transition energies, $\Delta E_{\mathrm{G}} = E_{\mathrm{G}}^{\mathrm{ct}} - E_{\mathrm{G}}^{\mathrm{g}}$, $\Delta \mathrm{E}_{\mathrm{CT}}^{\mathrm{g}} = \mathrm{E}_{\mathrm{CT}}^{\mathrm{g}} - \mathrm{E}_{\mathrm{CT}}^{\mathrm{ct}}$, $\Delta E_{\mathrm{A}^*} = E_{\mathrm{A}^*}^{\mathrm{ct}} - E_{\mathrm{A}^*}^{a^*}$, $\Delta \mathrm{E}_{\mathrm{CT}}^{\mathrm{a}^*} = \mathrm{E}_{\mathrm{CT}}^{\mathrm{a}^*} - \mathrm{E}_{\mathrm{CT}}^{\mathrm{ct}}$. Apart from the excitation energy, i.e., the energy required to change the molecular electronic state, the vertical transition energies include contributions related to the interaction of a molecule in a specific electronic state with the surrounding solvent. In a thermal equilibrium, motion of solvent molecules leads to fluctuations of the vertical excitation energies.[3, 4] If the corresponding energy distributions are Gaussian, the free energy profiles of diabatic states are parabolic and one can use the Marcus expression for the electron transfer reaction rate,

$$k_{\mathrm{ET}} = \frac{2\pi}{h\sqrt{4\pi\lambda k_{\mathrm{B}} T}} J^2 \exp\left[-\frac{(\lambda+\Delta G)^2}{4\lambda k_{\mathrm{B}} T}\right],$$

where ΔG is the driving force, or the free energy difference between the minima of diabatic states, i.e., $E_{\mathrm{G}}^{\mathrm{g}}$, $E_{\mathrm{CT}}^{\mathrm{ct}}$, and $E_{A^*}^{a^*}$ in our case, J is the electronic coupling element between them, and λ is the reorganization energy.

Averaged vertical excitation energies were calculated using the m062x range-separated functional and the 6-311g(d) basis set. Polarizable continuum model[5-7] was used to account for the solvent stabilization. All calculations were performed using the GAUSSIAN09 package.

The choice of the vertical excitation energies as a reaction coordinate is convenient for the evaluation of these quantities, in particular

$$\Delta G^{\mathrm{ct}\to\mathrm{g}} = \frac{1}{2}\left(\langle \Delta E_{\mathrm{G}}\rangle + \langle \Delta E^{\mathrm{g}}_{\mathrm{CT}}\rangle\right), \lambda^{\mathrm{ct}\to\mathrm{g}} = \frac{1}{2}\left(\langle \Delta E_{\mathrm{G}}\rangle - \langle \Delta E^{\mathrm{g}}_{\mathrm{CT}}\rangle\right)$$

$$\Delta G^{\mathrm{a}^*\to\mathrm{ct}} = \frac{1}{2}\left(\langle \Delta E^{\mathrm{a}^*}_{\mathrm{CT}}\rangle + \langle \Delta E_{\mathrm{A}^*}\rangle\right), \lambda^{\mathrm{a}^*\to\mathrm{ct}} = \frac{1}{2}\left(\langle \Delta E^{\mathrm{a}^*}_{\mathrm{CT}}\rangle - \langle \Delta E_{\mathrm{A}^*}\rangle\right),$$

where angular brackets denote mean values of the corresponding vertical excitation energies.

To evaluate (ensemble-averaged) vertical excitation energies, we used the polarizable continuum model (PCM). [5-7] We first performed geometry optimizations in the g, ct, and a* states at the m062x/6-31g(d) level of theory using DCM as an implicit solvent, saved the optimized solvent state, and then evaluated the excited state energies of other states in the saved (nonequilibrium) solvation shells.

Energy (Hartree)	**TT-Ph-PDI**	**T-(Ph)$_2$-PDI**	**T-(Ph)$_4$-PDI**
E_G^g	-5021.19893452	-7753.43700816	-8677.28997669
E_G^{ct}	-5021.12290884	-7753.36349869	-8677.21751102
E_{CT}^{ct}	-5021.18995581	-7753.42757525	-8677.28053133
E_g^{CT}	-5021.18660635	-7753.40266345	-8677.25271997
E_{A*}^{a*}	-5021.19095270	-7753.42764279	-8677.28011168
E_{CT}^{ct}	-5021.18664498	-7753.42757525	-8677.28053133
E_{CT}^{a*}	-5021.16941153	-7753.42673197	-8677.27886949
E_{A*}^{ct}	-5021.16121359	-7753.42058803	-8677.27296917

Energy (eV)	**TT-Ph-PDI**	**T-(Ph)$_2$-PDI**	**T-(Ph)$_4$-PDI**
$\Delta G_{\mathrm{ct}\to\mathrm{g}}$	1.04	0.66	0.61
$\lambda_{\mathrm{ct}\to\mathrm{g}}$	1.032	1.34	1.36
$\Delta G^{\#}_{\mathrm{ct}\to\mathrm{g}}$	6.4e-6	0.086	0.104
$\Delta G_{\mathrm{a}*\to\mathrm{ct}}$	0.003	0.085	0.08
$\lambda_{\mathrm{a}*\to\mathrm{ct}}$	0.063	0.11	0.1325
$\Delta G^{\#}_{\mathrm{a}*\to\mathrm{ct}}$	0.016	0.0012	0.0041

References

1 I. Howard, H. Mangold, F. Etzold, D. Gehrig and F. Laquai, *Journal*, 2013.

2 B. Fückel, A. Köhn, M. E. Harding, G. Diezemann, G. Hinze, T. Basche and J. Gauss, *J. Chem. Phys.*, 2008, **128**, 074505.

3 J. Blumberger, *Phys. Chem. Chem. Phys.*, 2008, **10**, 5651-5667.

4 T. Kowalczyk, L.-P. Wang and T. Van Voorhis, *J. Phys. Chem. B*, 2011, **115**, 12135-12144.

5 S. Miertuš, E. Scrocco and J. Tomasi, *Chemical Physics*, 1981, **55**, 117-129.

6 M. Cossi, V. Barone, R. Cammi and J. Tomasi, *Chem. Phys. Lett.*, 1996, **255**, 327-335.

7 J. Tomasi, B. Mennucci and R. Cammi, *Chem. Rev.*, 2005, **105**, 2999-3094.